UNIVERSITY OF CALIFORNIA, SAN DIEGO

Photovoltaic Roof Heat Flux

A Thesis submitted in partial satisfaction of the requirements
for the degree Master of Science

in

Engineering Sciences (Mechanical Engineering)

by

Mezhgan Frishta Samady

Committee in charge:

Professor Jan Kleissl, Chair
Professor Larry Armi
Professor James Rottman

2011

The Thesis of Mezhgan Frishta Samady is approved and it is acceptable in quality and form for publication on microfilm and electronically:

_____

_____

_____
Chair

University of California, San Diego

2011

DEDICATION

For the girls in the Afghanistan who risk their lives for an education while I have the freedom to learn more. Little do they realize I get my strength from them.

For my parents and my family, thank you for all your love and support in everything that I do! ☺

EPIGRAPH

"I have accepted fear as a part of life, specifically the fear of change. I have gone ahead despite the pounding in the heart that says turn back."

— Erica Jong

TABLE OF CONTENTS

SIGNATURE PAGE.....iii

DEDICATION..... iv

EPIGRAPH..... v

TABLE OF CONTENTS..... vi

LIST OF ABBREVIATIONS ix

LIST OF FIGURES..... xi

LIST OF TABLES..... xvii

ACKNOWLEDGEMENTS..... xviii

ABSTRACT OF THE THESIS xix

1. INTRODUCTION..... 1

2. METHODS..... 4

2.1. Heat Transfer Analysis 4

2.1.1. Basic Thermodynamics and Assumptions 4

2.1.2. Building Heat Transfer 5

2.1.3. Heat Transfer of Units 6

2.2. Experimental Setup and Data Collection..... 10

2.2.1. Testing Location 10

2.2.2. Building Models 12

2.3. Modeling for Heat Flux Equations 13

2.3.1. Crank-Nicholson for temperature Layers 13

2.3.2. Longwave (IR) radiation 15

2.3.3. Convection 15

2.3.4. Exposed Roof Temperature 16

2.4. Seasonal Temperature Modeling 17

2.5. Calibration and errors 20

3. RESULTS 22

3.1. Setup #1 22

3.2. Setup #2 27

3.3. Cooling Load Comparison 32

3.4. Seasonal Modeling 35

3.4.1. Modeling- Exposed Roof 35

3.4.2. Modeling –Back Panel 38

3.4.3. Summer Heat Flux 40

4. DISCUSSION AND CONCLUSIONS 42

BIBLIOGRAPHY 47

APPENDIX 49

A. HVAC unit 49

B. 1D vs. 2D heat transfer validation 49

C. Details of Heat Flux Formulas 51

i. Offset 51

ii. Angled 51

iii. Flush 52

D. Inside the Units 53

E. Albedo Test 54

F. Details of Setup #1 54

G. Details of Setup #2 60

H. Modeled Tpv from A.D. Jones: 65

I. Modeled Temperatures using Actual Values 66

J. HVAC Operation 67

K. PVWatts Calculations 68

LIST OF ABBREVIATIONS

Symbol/ Abbreviation	Description
Subscripts	
a, c, f 3,2,1	angled, control, flush designs (relatively)
PV	Photovoltaic Solar Panel
atm, ∞	Atmosphere
c, r, r2	ceiling, back panel roof, exposed roof
I	inside unit
G	gap between panel and roof
Air	Relative air at z=129.2 m

Symbol/ Abbreviation	Description	Source
Variables		
Sd	Downward Shortwave Radiation	Radiation sensor
Ld	Downward Longwave Radiation	CIMIS
Su	Upward Shortwave Radiation	Appendix C
Lu	Upward Longwave Radiation	Appendix C
Σ	Stephen-Boltz constant	5.67×10^{-8} W/m^{2}K^4
P	Density	roof= 630 kg/m^3 air= 1.204 kg/m^3
ϵ	Thermal Emissivity	roof= 0.96 pv = 0.95
GHI	Global Horizontal Irradiance	LiCor pyrometer
K	Thermal Conductivity	roof= 0.13 W/mK air= 0.025 W/mK
H	Convection Coefficient	Section 2.3.3
G, H	Conduction, Convection	Appendix C
Q_{out}	Heat Extracted from building (Cooling load)	(1) (Section 2.1.1)
T	Temperature	T107L (air), Thermistor (Surface)
Tr_2	Temperature of Exposed Roof	Thermistor/ RIMAC Surface

Symbol/ Abbreviation	Description	Source
Cp	Specific Heat Constant	roof= 1300 kJ/kgK air=1003.5 J/kgK
A_x	Area	Back panel: c, f= 0.1863 m^2 a = 0.1613 m^2 Exposed: 1, 2= 0.1027 m^2 3= 0.1272 m^2
A	Roof Albedo	0.36 (Appendix E)
ALB	Shortwave Radiation under panel	K&Z pyranometer
l	Thickness	roof = 0.111 m gap= 0.0254 m
A	Terrain Roughness Coefficient	1, 2 , 3 =0.25 c = 0.15
ß	Terrain Roughness Coefficient	1, 2, 3 = 0.67 c = 1.0
C_H	Bulk Heat Transfer Coefficient	0.05

LIST OF FIGURES

Figure 1: Illustration of the thermodynamic system. 5

Figure 2: a) Photograph of the flush unit. b) Schematic with heat fluxes ... 7

Figure 3: a) Photograph of the offset unit. b) Schematic with heat fluxes... 8

Figure 4: a) Photograph of the angled unit. b) Schematic with heat fluxes. 9

Figure 5: Google image of RIMAC roof. 10

Figure 6: Setup #1 on RIMAC roof. 11

Figure 7: Setup #2 on RIMAC roof. 12

Figure 8: a) Relationship between surface temperature of RIMAC and the exposed roof temperature 17

Figure 9: a) [left] Modeled temperature of offset air gap 19

Figure 10: Example of linear regressions performed for calibrating the thermistors 21

Figure 11: Linear calibration regressions for K&Z pyranometers. 21

Figure 12: a) Wind speed of the DEMROES weather station during the 3.5 day test of setup #1. b) GHI measured from the DEMROES weather station during the test of setup #1 22

Figure 13: Measured temperatures of setup #1 over 3.5 days 24

Figure 14: For setup #1 - a) & c) temperatures through the roof under the panel; b) & d) temperatures through the roof of the exposed area. 25

Figure 15: Modeled heat fluxes for the offset (control) unit..... 26

Figure 16: Collective heat fluxes for the flush unit..... 27

Figure 17: a) Wind speed of the DEMROES weather station during the 3.5 day test of setup #2. b) GHI measured from the DEMROES weather station during the test..... 28

Figure 18: Measured temperatures of setup #2 over 3.5 days..... 29

Figure 19: For setup #2 - a) & c) temperatures through the roof under the panel; b) & d) temperatures through the roof of the exposed area. 30

Figure 20: Collective heat fluxes for the offset unit during setup #2 test.. 31

Figure 21: Collective heat fluxes for the angled unit during setup #2 test. 31

Figure 22: a) Modeled temperature of exposed roof $\boldsymbol{Tr2, c}$..... 35

Figure 23: a) Modeled temperature of exposed roof $\boldsymbol{Tr2, f}$..... 36

Figure 24: a) Modeled temperature of exposed roof $\boldsymbol{Tr2, a}$ 36

Figure 25: a) Modeled temperature of roof under the solar panel $\boldsymbol{Tr, c}$..... 38

Figure 26: a) Modeled temperature of roof under the solar panel $\boldsymbol{Tr, f}$ 39

Figure 27: a) Modeled temperature of roof under the solar panel $\boldsymbol{Tr, a}$ 40

Figure 28: Performance curve of the HVAC unit- TECA 150-HP CP..... 49

Figure 29: A photo of the setup to compare the 1-dimensional heat flux and 2-dimensional heat flux..... 50

Figure 30: Normalized upward longwave radiation heat flux from roof for the 1D and 2D cases..... 50

Figure 31: A visual inside the units..... 53

Figure 32: Albedo test..... 54

Figure 33: All the temperatures of the control unit for setup #1..... 54

Figure 34: All the temperatures of the flush unit for setup #1..... 55

Figure 35: Battery voltage for both units of Setup #1..... 55

Figure 36: Radiation sensors for both units in comparison to GHI during testing days of Setup #1. 56

Figure 37: Conductive Heat flux in the first roof layer for both units of Setup #1 56

Figure 38: Energy balance of the second control volume from Figure 3 for the control unit of setup #1. 57

Figure 39: Energy balance of the second control volume from Figure 2 for the flush unit of setup #1. 57

Figure 40: Comparison of the convective heat flux of the first control volume for the units of setup #1. 58

Figure 41: Comparison of the longwave radiation from the atmosphere (and solar panel for the control unit) from the first control volume for the units of setup #1. 58

Figure 42: Comparison of the longwave radiation from the units of setup #1 up towards the atmosphere. 59

Figure 43: Comparison of the net shortwave heat flux of the first control volume for the units of setup #1. 59

Figure 44: All the temperatures of the control unit for setup #2. 60

Figure 45: All the temperatures of the angled unit for setup #2. 60

Figure 46: Battery voltage for both units of Setup #2 during the 3.5 day test. 61

Figure 47: Comparison of the radiation sensor measurements for both units in during the testing days of Setup #2. 61

Figure 48: Conductive Heat flux in the first roof layer for both units of Setup #2. 62

Figure 49: Energy balance of the second control volume from Figures 3 for the control unit of setup #2. 62

Figure 50: Energy balance of the second control volume from Figures 4 for the angled unit of setup #2. 63

Figure 51: Comparison of the convective heat flux of the first control volume for the units of setup #2. 63

Figure 52: Comparison of the longwave radiation from the atmosphere (and solar panel for the control unit) from the first control volume for the units of setup #2 64

Figure 53: Comparison of the longwave radiation from the units of setup #2 up towards the atmosphere..... 64

Figure 54: a) Modeled panel temperatures for the control unit compared to the actual 65

Figure 55: a) Modeled panel temperatures for the flush unit compared to the actual 65

Figure 56: a) Modeled panel temperatures for the angled unit compared to the actual 65

Figure 57: Modeled exposed rooftop temperatures for the control unit compared to the actual using the actual values of Tg, Tr_2 and Tp (as opposed to modeled temperatures). 66

Figure 58: Modeled exposed rooftop temperatures for the angled unit compared to the actual using the actual values of Tg, Tr_2 and Tp (as opposed to modeled temperatures). 66

Figure 59: Operation of HVAC system for the offset (control) and flush units 67

Figure 60: Operation of HVAC system for the offset (control) and angled units 67

Figure 61: Calculation of PVWatts energy output produced by the angled solar panel 68

Figure 62: Calculation of PVWatts energy output produced by the flush and offset solar panels..... 68

LIST OF TABLES

Table 1: Tests conducted for design comparison 11

Table 2: Modeled temperatures based off design. 18

Table 3: Average power draw (work) of the HVAC system for the offset (control) and flush units during first 3 days of Setup #1..... 33

Table 4: Average power draw (work) of the HVAC system for the offset (control) and angled units during first 3 days of Setup #2..... 34

Table 5: Total energy usage by HVACs for both setups in Wh..... 34

Table 6: Conduction heat flux through roof of units 41

Table 7: Total energy charges for the different solar panel designs for both Setup #1 and Setup #2. 45

Table 8: Properties of the High Density OSB Particleboard..... 53

ACKNOWLEDGEMENTS

I would like to thank Professor Jan Kleissl for his support as the chair of my committee. With his wisdom, willingness to help, dedication to science, and sense of humor, I was able to pursue my degree. I'd also like to thank Professor Kleissl's PhD student, Anthony Dominguez, for spending many of hours working with me during analysis and modeling.

I would like to acknowledge David Purtell and Millie Mcmilion for allowing me to use RIMAC roof as my testing facility. I would like to express my appreciation to Dave and Nick for their assistance while I was in the machine shop and other hands on needs. And finally, many thanks to Rick Driscoll, Andrea Cardenas, Rocky Rosenow, Tyler Dill and Louis Topper from MAE 171B for their great work in getting this project rolling.

ABSTRACT OF THE THESIS

Photovoltaic Roof Heat Flux

by
Mezhgan Frishta Samady

Master of Science in Engineering Sciences (Mechanical Engineering)

University of California, San Diego, 2011

Professor Jan Kleissl, Chair

Solar panels were mounted with different designs onto 1:800 scale building models while temperature and radiation were measured. While there have been other studies aimed at finding the optimal angles for solar panels [9], in this study both the angle and the mounting method were tested. The three PV mounting designs that were considered to provide the most insulation to a building's rooftop were flush, offset (control), and angled. The solar panel offset height became a key component for rooftop insulation as well as the performance of the actual solar panel. Experimental results were given to verify the thermal behavior of the heat loads from the different designs of the photovoltaic panel. From the results, the angled PV design needed 16% more heat extraction than the offset and flush PV design needed 60% more heat extracted than the offset. In addition to the heat transfer analysis, thermal models were performed to incorporate main atmospheric conditions which were based on the effects of PV mounting structure.

1. INTRODUCTION

There is a recent interest to improve energy efficiency and create new 'zero' emission energy sources. The main purposes are to decrease energy costs and abandon conventional fossil fuel energy generation to reduce greenhouse gas emissions. Economic incentives and a commitment to preserving the environment have attracted people to solar energy. Even on a state level, California's Air Resources Board proposed a target of 33% Renewable Portfolio Standard (RPS) by 2020 in order to achieve AB 32 goals [4]. It is the responsibility of investor-owned utilities (IOUs) to achieve this goal. In addition, the California Public Utilities Commission (CPUC) has established incentive programs such as the California Solar Initiative (CSI) to entice consumers to install solar photovoltaic devices (PV). The results of these programs are that many residents and business owners are "going solar" for their electric and water heating needs [11].

In general, buildings use about 40% of the energy in urban areas [15] and a major factor of energy usage (~37%) is the amount of Heat, Ventilation, and Air Conditioning (HVAC) in the buildings. HVAC energy use is a result of heating loads on the building including: air conditioning of outside air being moved into the building to improve air quality, conduction of heat through the building envelope which is heated by solar radiation, and internal heat loads such as computers, people, and office equipment. Reducing a HVAC systems energy use has the potential to decrease the demand of energy, which also decreases the amount of anthropogenic heat released in the environment. This is especially

important in areas with hot climates such as Southern California where it takes more work to keep buildings at a comfortably cooler temperature.

There have been several design approaches to reduce energy usage in order to cool buildings. Radiation on a building's surface, particularly in sunny southern US cities, has an influence on the amount of air conditioning usage. There have been attempts to increase a roof's albedo (or solar reflectance) by painting the rooftops white or provide shading by planting trees around the building. While these approaches have proven to be somewhat effective [1], new studies show that building integrated photovoltaics (BIPV) could also reduce cooling load [18]. BIPV takes into effect how the solar panel will influence the building the PV is mounted upon. The future implementation of BIPV could potentially replace conventional building elements such as roof tiles, asphalt shingles, facade elements, and shading devices [19].

The major questions in this research study were: how does the design of PV panels on roofs impact cooling load in buildings and could the heat transfer processes be modeled to estimate the effects for different solar panel designs and times of year? This project examined both BIPV-type panels that are part of the building structure, and 'add-on' PV panels that are placed on top of the existing roofs with room for convection of heat from the back of the panel. PV panels are already beneficial because they are a clean, renewable source of energy; an added benefit could be their insulation effects on buildings.

In a recent study, PV panel insulation effects were measured off the coast of Madagascar in La Reunion Island [3]. Bigot's study found that mounting PV panels on building roofs reduced the interior ceiling temperature by up to 6°C

compared to a building with no PV panel. Their analysis showed that a solar panel over a rooftop will lead to a reduction of cooling loads by up to 51% relative to a roof with no panels. These measurements indicate that in general PV panels are a source of insulation and an added benefit to traditional insulators.

The prime goal of this work was to build an accurate computational model for building roof heat transfer with solar panels. Building energy and HVAC modeling programs, such as Energy Pro, do not take into account the impacts that solar panels have on the heat transfer of a rooftop. Careful modeling of the roof and building will provide the information to compute the heat flux through a roof. The significant factor of the heat flux into a building was the rooftop temperature [3]. Holistic approaches to modeling heat flux require computational methods and experimental data from rooftops of different PV positions. Our objective was to be able to build and calibrate a computation model to estimate the impact of solar PV on roof cooling load. With the growth of urban PV installations, such a tool can help with PV design considerations and estimate the associated building HVAC energy savings.

The next couple of sections of the thesis will go through the setup and the different considerations for the project, as well as a background of the theory. Subsequent to the methods, the results of the experiments will be discussed and plots provided for comparison. From there, based off the results, conclusions and suggestions for further studies will be made.

2. METHODS

This section will begin by analyzing the theory behind the thesis. Afterwards, the experiments and heat transfer formulas are introduced with figures of the experimental setups. In addition, the different computational methods used in the project are discussed as well as calibrations of the equipments.

2.1. Heat Transfer Analysis

2.1.1. Basic Thermodynamics and Assumptions

The second law of thermodynamics states that heat cannot flow from a cold reservoir to a warm reservoir spontaneously without work. In classical thermodynamics, the second law is a basic axiom applicable to any system involving heat transfer (Figure 1). In this project, an air conditioner with a refrigeration cycle was used, where heat from inside the units ('source') was moved to the outside ('sink') when the set point inside air temperature was reached. The heat energy was removed (i.e. cooling load) by a mechanism where work was applied to a HVAC system operating a gas cycle. The components corresponding to the condenser and evaporator in a vapor compression cycle are the hot and cold gas-to-gas heat exchangers in the HVAC.

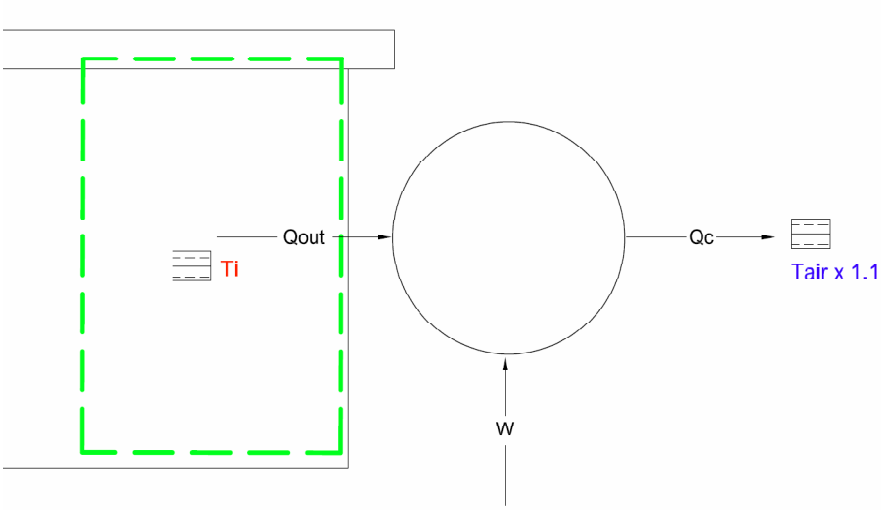

Figure 1: Illustration of the thermodynamic system. Heat (Qout) is removed from the inside of the building at temperature T_i. The heat Q_C = Qout + W is released into the outside air T_{air}. The green control volume corresponds to the green control volumes of Figure 2b. 3b, and 4b

Q_{out} is defined as the extracted heat out of the building to maintain the set point temperature. Equation (1) was given by the HVAC manufacturer to calculate Q_{out} in Watts as the performance curve, which can be seen in the Appendix [14].

$$Q_{out} = \frac{1}{1.5692}[T_i - (T_{air} \cdot 1.1)] + 42.5 \quad (1)$$

The temperature difference for Q_{out} is the difference between where the HVAC unit removed the air (Ti) to where the air was released, which was assumed to be 1.1 x T_{air}.

2.1.2. Building Heat Transfer

The modes of heat transfer involved in this project were conduction, convection and radiation. For a thin control volume of a horizontal surface, the basic heat transfer balance was the sum of the conduction and convection equaling the net radiation. Net radiation is defined as the sum of all incoming and outgoing fluxes of shortwave radiation (solar radiation), which came from the

sun, and longwave or thermal infrared radiation. During the daytime, heat would enter the roof by conduction creating a positive heat flux into the buildings, while convection and the HVAC would create a negative heat flux and remove the heat.

Each of the experimental setups used in this project (Section 2.2) had distinct heat transfer equations. However, some heat transfer fluxes were the same for all the setups, mainly those from the atmosphere. Equation (2) was the formula used to calculate the shortwave radiation down to the units (Sd_{atm}) from the atmosphere, which was the Global Horizontal Irradiance (GHI) measured from the weather station multiplied by the area that is exposed to the roof (A), based on the panel design.

$$Sd_{atm} = GHI \cdot A \tag{2}$$

Atmospheric longwave radiation down to the units (Ld_{atm}), which is a function of temperature, was also a common heat flux in the units. The basic equation was

$$Ld_{atm} = \epsilon_{atm} \cdot \sigma \cdot {T_{atm}}^4 \cdot A \tag{3}$$

Since the temperature and emissivity of the atmosphere were difficult to measure, a different approach of how the longwave radiation was calculated is explained in Section 2.3.2. Description of the abbreviations in these formulas can be found in the Table of Abbreviations.

2.1.3. Heat Transfer of Units

PV panel placement can be broken down into three variables: the panel tilt, its offset from the roof, and aspect ratio of panel to roof. The "control" (Figure 3) of the experiments was a building with a solar panel at an offset of 0.076m, which

is ideal in keeping the PV panel temperature adequate for the largest efficiency [7]. The flush panel (Figure 2) was caulked onto the building to ensure that there was no air leakage between the panel and the roof. The heat transfer control volumes for the offset and flush units are illustrated in figures 3b and 2b. The abbreviations are defined in the Table of Abbreviations and the buildings will be discussed in Section 2.2.2.

a)  b) 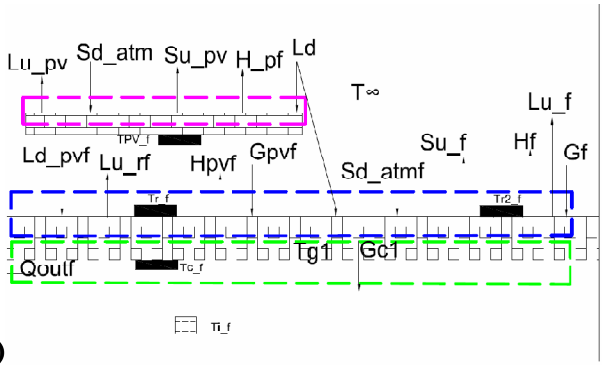

Figure 2: a) Photograph of the flush unit. b) Schematic with heat fluxes and temperature sensors. For the analysis, only the roof surface (blue) and ceiling surface (green) CVs were calculated. The lateral fluxes at the boundary of the CVs were ignored.

$$0 = Ld \cdot A_1 + Ld_{pv,f} + Sd_{atm,f} - \left(Lu_f + Lu_{r,f} + Su_{atm,f}\right) - \left(G_f + G_{pv,f} + H_f + H_{pv,f}\right) \quad (4)$$

$$0 = Qout_f - G_1^* - G_{pv,1}^* \quad (5)$$

In order to analyze the heat transferred through the roofs, two control volumes (CV) were defined. For both designs, the first equations (4 and 6) represented energy conservation for the rooftop (blue) control volume and second (5 and 7) represented energy conservation for the interior (green) control volume respectively. The main differences between the heat flux equations in the offset unit (6 and 7) versus the flush unit (4 and 5) were the type of convection and the short wave radiation underneath the solar panel. The flush unit experienced a

natural convection under its solar panel with diffuse radiation as opposed to shortwave radiation. Underneath the offset panel there was forced convection and short wave radiation, however the shortwave radiation would be minimum when the sun was perpendicular to the roof. Further details of their heat flux equations can be found in Appendix Ci and Ciii.

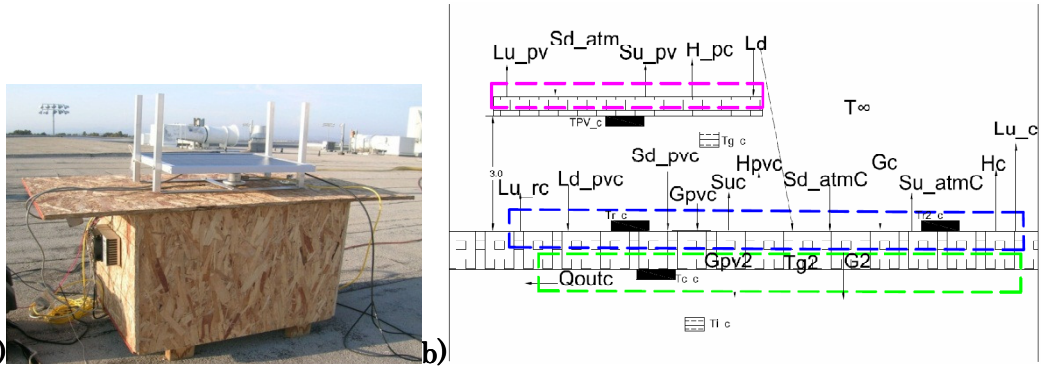

Figure 3: a) Photograph of the offset unit. b) Schematic with heat fluxes and temperature sensors. For the analysis, only the blue and green CV's were calculated.

$$0 = Ld \cdot A_1 + Ld_{pv,c} + Sd_{atm,c} + Sd_{pv,c} - \left(Lu_c + Lu_{r,c} + Su_{atm,c} + Su_c\right) - (G_c + G_{pv,c} + H_c + H_{pv,c}) \quad (6)$$

$$0 = Qout_c - {G_2}^* - {G_{pv,2}}^* \quad (7)$$

Solar panels often are tilted to be closer to the perpendicular of a solar beam radiation in order to produce more energy. This tilt can also help in reducing the temperature of the panels by increasing convective heat transfer on both sides of the panel [10]. The effect of this convection could improve PV performance depending on the temperature of the surrounding air and the temperature coefficient of the solar panel. On the other hand, the increased shortwave radiation reaching the roof from the sides of the panel can create an increase in the roof downward heat flux. This increase in shortwave radiation is

a function of the offset height of the solar panel. Figure 4 gives a pictorial view of the angled solar panel as well as the heat transfer fluxes. The associated equations for the angled unit (8 and 9) are for the roof surface control volume (blue) and ceiling surface control volume (green) respectively. Details of the angled heat transfer formulas are in Appendix Cii.

a) 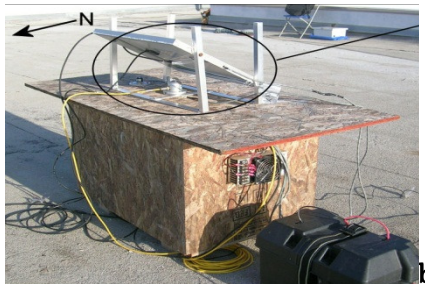

b) 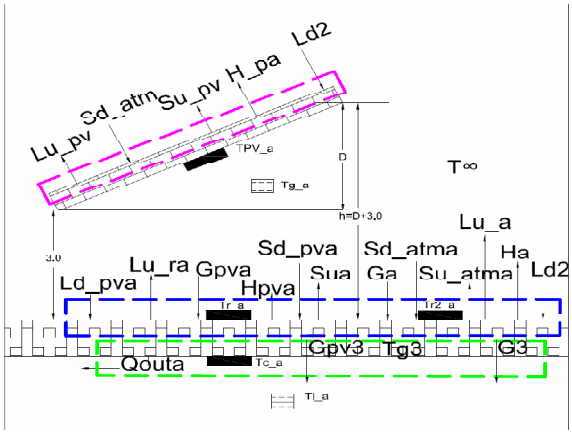

Figure 4: a) Photograph of the angled unit. b) Schematic with heat fluxes and temperature sensors. For the analysis, only the blue and green CV's were calculated.

$$0 = Ld \cdot A_3 + Ld_{pv,a} + Sd_{atm,a} + Sd_{pv,a} - \left(Lu_a + Lu_{r,a} + Su_{atm,a} + Su_a\right) - (G_a + G_{pv,a} + H_a + H_{pv,a}) \quad (8)$$

$$0 = Qout_a - {G_3}^* - {G_{pv,3}}^* \quad (9)$$

The angled panel heat transfer equations are very similar to the offset panel because the designs were the same, aside from the tilt in the panel. Underneath the panel was forced convection and the shortwave radiation was also at its minimum during the middle of the daytime. However, one significant difference between the offset and angled unit in the heat transfer equations was the calculation of the areas. The tilt of the panel made the area of the solar panel shadow on the roof (Apv_a) less than the shadow area from the offset or flush panels (see Abbreviation Table).

Since all the designs had an area exposed to the atmosphere and an area unexposed, there was an assumption that the roof heat fluxes varied in two dimensions. The validation of this assumption is discussed in Appendix B.

2.2. Experimental Setup and Data Collection

2.2.1. Testing Location

In order to conduct proper analysis, it was necessary to measure the environment/weather that the models were placed in. UCSD campus has eight different Decision Making Using Real-time Observations for Environmental Sustainability (DEMROES) stations all around campus, one of which included the RIMAC gymnasium roof (Figure 5). The measurements that were taken from the DEMROES station included GHI, wind speed, air temperature, relative humidity, and RIMAC surface temperature (when necessary) at 5 minute averages. Another advantage of using the RIMAC roof as a testing area was there was no shading effects that would obstruct the tests. Also, for this reason, the units were placed at a distance far enough from each other to minimize shading affects.

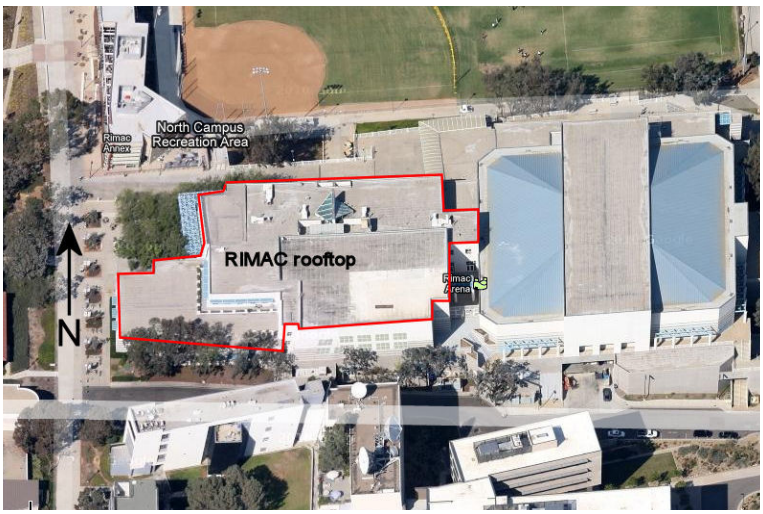

Figure 5: Google image of RIMAC roof. Mean sea level = 129.2m, Latitude= -117.25°, Longitude= 32.9°.

Two main tests were conducted on the units. Experimental time and weather conditions are shown in Table 1. The dates were during the month of September and were chosen because they represent the generally warm and dry weather in Southern California where the HVAC system would be actively utilized. Data from the units was taken at 5 minute averages for consistency with the DEMROES data.

Table 1: Tests conducted for design comparison

Setup #	Start date & time	End date & time	Average Air temp	Inside control temp
1	09/21/10 - 00:00	09/24/10- 10:35	16.62°C	21.5°C
2	09/09/10 - 00:00	09/12/10 - 09:20	17.18	21.5°C

In setup #1 (Figure 6), the offset panel (control) was compared to a building consisting of a flush solar panel (Figure 2). The main goal of this setup was to test the effects of natural convection versus forced convection heat transfers from the wind underneath the solar panels.

Figure 6: Setup #1 on RIMAC roof. Weather station on the left, offset (control) unit in the middle, and flush on the right.

In setup #2 (Figure 7), the offset acted as the control again and was now compared to the tilted solar panel at the same offset of 0.076m (Figure 4). The solar panel tilt angle was 32.6° and was towards the south which is common on

buildings for standard performance of a solar panel [10]. Essentially, this setup was to test the effects of sun exposure to the roof and its affect to the heat transfer.

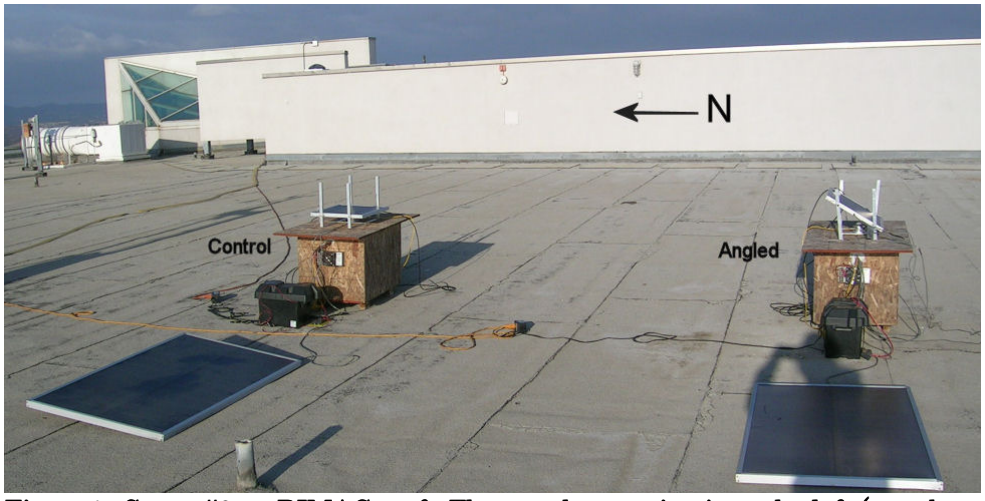

Figure 7: Setup #2 on RIMAC roof. The weather station is to the left (not shown), offset (control) unit in the middle, and angled PV on the right.

2.2.2. Building Models

The building models were composed of two identical small scale buildings of the same dimension and envelope properties. The material used to build the models was 0.011m oriented strand board (OSB) which is commonly used to construct residential homes and buildings (Appendix D). The dimension of the buildings were 0.406m x 0.711m x 0.452m and roof dimensions were 1.219m x 0.609m, leaving a 0.254m over hang on one side and a 0.127m over hang on the other. Since the focus of heat transfer was the roof, the overhangs were designed to shade and minimize the heat transfer through the sides (or walls). In order to decrease the heat transfer through the walls and the floor of the models, R-13 insulation was used to insulate the walls (as commonly used in residential buildings) and the structure was offset from the ground using legs. The R-13,

with a resistive value of 24.6 K/W (13°F*hr/BTU), insulated important factors such as wind speed and air temperature from affecting the model's wall temperatures. The purpose of the legs under the models was to reduce the conductive heat transfer from the ground (in this case RIMAC roof surface) to the buildings.

To create a sealant for the models so that no outside air entered the building, the corners, wire holes, and sides of the building were caulked, as well as the roof to the building. In order to eliminate the often dominating contribution of solar gains, the models had no windows. The air conditioning unit was used to keep the buildings at a moderate temperature so the inside room temperature was not a factor in the ceiling temperature and, in turn, the heat flux through the roof. The HVAC unit was able to maintain the set temperatures of the buildings through a control system involving a relay switch. Essentially, given steady state conditions, the amount of heat that was extracted from each of the models demonstrated the heat flux through the building with the particular PV design.

The solar panels in this study were Uni-Solar panels, 0.489m x 0.381m in size, which created approximately a 1:4 ratio with the rooftop of the models. This solar panel size was chosen because the ratio to rooftop area was similar to actual rooftops.

2.3. Modeling for Heat Flux Equations

2.3.1. Crank-Nicholson for temperature Layers

The control volume sketches from Section 2.1.3 showed that the conduction heat flux through the roof was a one dimensional transient heat

transfer model. This required the roof of the building units to be divided into different areas for conduction calculations. The boundary conditions were the measured rooftop temperature and the inside ceiling temperature. Since latent heat flux was assumed to be zero [18], the equation for the sensible heat flux was used

$$\rho c_p \frac{\partial T}{\partial t} = k \frac{\partial^2 T}{\partial x^2} \tag{10}$$

In order to conduct these calculations, computational methods were necessary. Dominguez developed a computation for this application using the Crank-Nicholson numerical methods of discretization with even layers of the roof's length [6]. The number of layers was chosen by Dominguez through a sensitivity analysis for a roof which found that the method worked best using powers of 2 and the most optimal number of layers was 32. The properties of the wood for this calculation are in Table 8 (Appendix D). For each of the designs, the conduction in the blue CV (Figures 2, 3, and 4) (11) was calculated using the difference between the roof and the first designated layer of the Crank- Nicholson method while the green CV (12) used the last layer and the ceiling.

$$G_{pv} = \left(\frac{A_{pv}}{l}\right) \cdot k_{roof} \cdot (T_r - T_{1r}) \tag{11}$$

$$G_{pv\,2} = \left(\frac{A_{pv}}{l}\right) \cdot k_{roof} \cdot (T_{32} - T_s) \tag{12}$$

The Crank-Nicolson method was also used for calculating the natural convection under the flush panel. The measured air temperature between the solar panel and the roof would have been ideal for calculating convective heat fluxes; however, placing an air temperature sensor under the flush panel was difficult in order to guarantee there would be no air flow leakage. The boundary

conditions for this calculation were the temperature of the solar panel and the roof temperature. For the actual convective heat flux calculation, the last two layers of the 32 Crank-Nicholson values were used.

2.3.2. Longwave (IR) radiation

Longwave radiation from the atmosphere was calculated using a formula developed by the California Irrigation Management Information System (CIMIS)

$$Ld = (f\epsilon_{net} - \epsilon_{roof}) \cdot \sigma \cdot {T_{air}}^4 \quad (13)$$

The CIMIS calculation took the Stephen Boltzman's formula and used the ratio between measured GHI and clear sky GHI to calculate f, the cloud fraction. Relative humidity and the air temperature were used to calculate the vapor pressure which estimated the net sky emissivity

$$\epsilon_{net} = 0.34 - 0.14 \cdot \sqrt{e_a} \quad (14)$$

2.3.3. Convection

The convection coefficient was determined by splitting it into the forced and natural convection [16].

$$h_c = h_n + h_f \quad (15)$$

The natural convection was calculated by using ASHRAE's Handbook of Fundamentals [2]. The forced convection component differed per setup.

For the exposed roof next to the solar panels that had an offset (in this project the offset and angled units), a correlation method was used to calculate h_f [13]. With R_f= 2.17, W_f = 1.0, and the modified wind speed (α and ß are in the Abbreviation Table) considered to be at the same height as the weather station [17], h_f can be calculated as

$$h_f = 2.537 \cdot W_f R_f \sqrt{\frac{PV}{A}} \quad (16)$$

The exposed area of the flush panel design was slightly different because there was no wind flow under the panel nor as much shading. With this design, h_f was calculated using the same formula (16) but a different R_f of 1.13.

For the area under the offset unit's solar panel, the h_f formula (16) was again used. For this case, $R_f$and W_f were the same as the exposed offset unit, instead the α and ß of the modified wind speed formula differed (Abbreviation Table). The h_f for the area under the angled unit varied from the rest of the convection coefficients as

$$h_f = \rho \cdot c_p \cdot u \cdot C_H \quad (17)$$

where the density and heat capacity are for air, and C_H is the non-dimensional bulk heat transfer coefficient, ranging from 0.002 -0.02 for smooth to rough surfaces.

2.3.4. Exposed Roof Temperature

During the tests, there was only one thermistor on the roof which was directly underneath the solar panel, and the temperatures of the roof that was not exposed by the solar panel was also necessary for the heat transfer analysis. For this reason, a separate test was conducted where temperature measurements of a completely exposed roof were taken to estimate the temperature of the exposed roof during setups #1 and #2. The Least Squares method was then used to correlate a linear fit between the exposed unit's roof and the surface temperature of RIMAC roof (Figure 8).

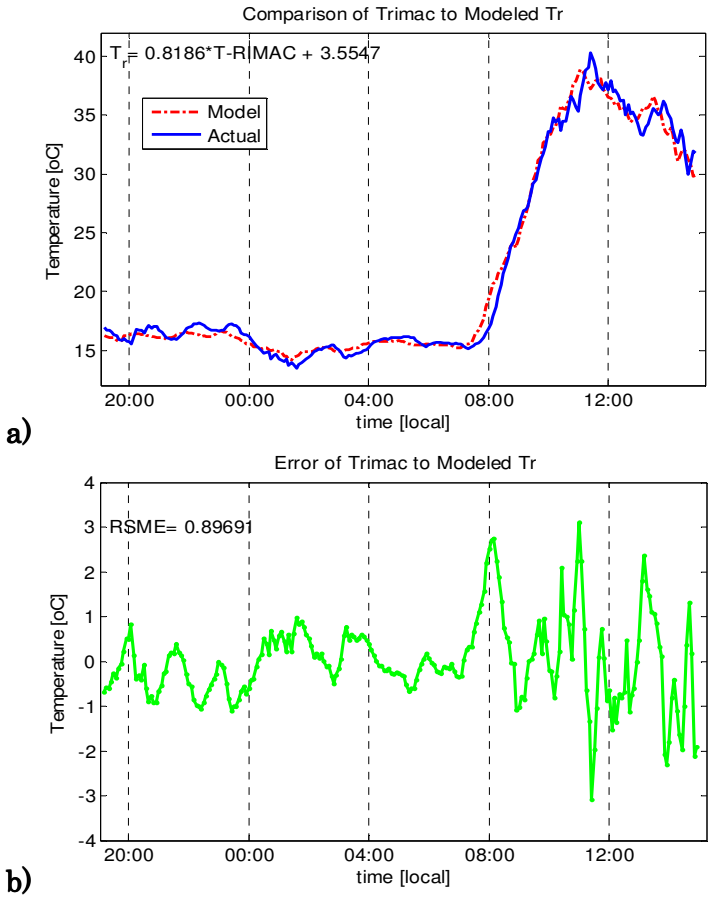

Figure 8: a) Relationship between surface temperature of RIMAC and the exposed roof temperature b) Error of the relationship with an RMSE of 0.897. This relationship was assumed to be linear and is used in the tests to calculate the temperature of the exposed roof not covered by the panel.

2.4. Seasonal Temperature Modeling

The key objective of this project was to develop and calibrate heat transfer models to be able to simulate annual temperatures, heat fluxes, and energy use. With modeled temperatures, it will be possible to predict how a building reacts to other seasons and locations with varying environmental conditions. The modeled temperatures for each individual unit for a period of time could be further analyzed for heating or cooling loads. The first part to modeling was to decide which inputs would be available to drive the model. Since the California Solar Initiative (CSI) program requires some consumers to provide the solar panel

energy production, many solar installations have basic weather stations. With the T_{air}, GHI, wind speed, and relative humidity given from this weather station, the temperatures that need to be simulated for each of the designs are given in Table 2.

Table 2: Modeled temperatures based off design. Locations of these temperatures were shown in Figures Cb, Bb, and Eb.

Design	Modeled temperatures
Offset	T_{pv}, T_g, T_r, Tr_2
Flush	T_{pv}, T_r, Tr_2
Angled	T_{pv}, T_g, T_r, Tr_2

Since the meteorological forcing impacts the buildings from the top and penetrates through the different layers, the first temperature to model was T_{pv}. Jones and Underwood developed a model based on the thermal load of a PV panel [Jones- 2006]. For the T_{pv} model, it was assumed that T∞ was a linear function relative to the temperature of the air. Also, the authors left the forced convection coefficients dependent upon to the reader to obtain an optimal value. Analysis of the T_{pv} method as well as RMS graphs can be found in Appendix H.

Since there was no air temperature sensor between the solar panel and the roof for the flush design, it was only necessary to model this gap temperature (T_g) for the offset and angled designs. In the case of the gap temperature, the assumption was that there was a (statistical) linear multivariate relationship between the temperature of the air gap with the wind speed, shortwave radiation, temperature of the air, and T_{pv}. Since our model was to be linear, Least Squares method was again used (Figure 9).

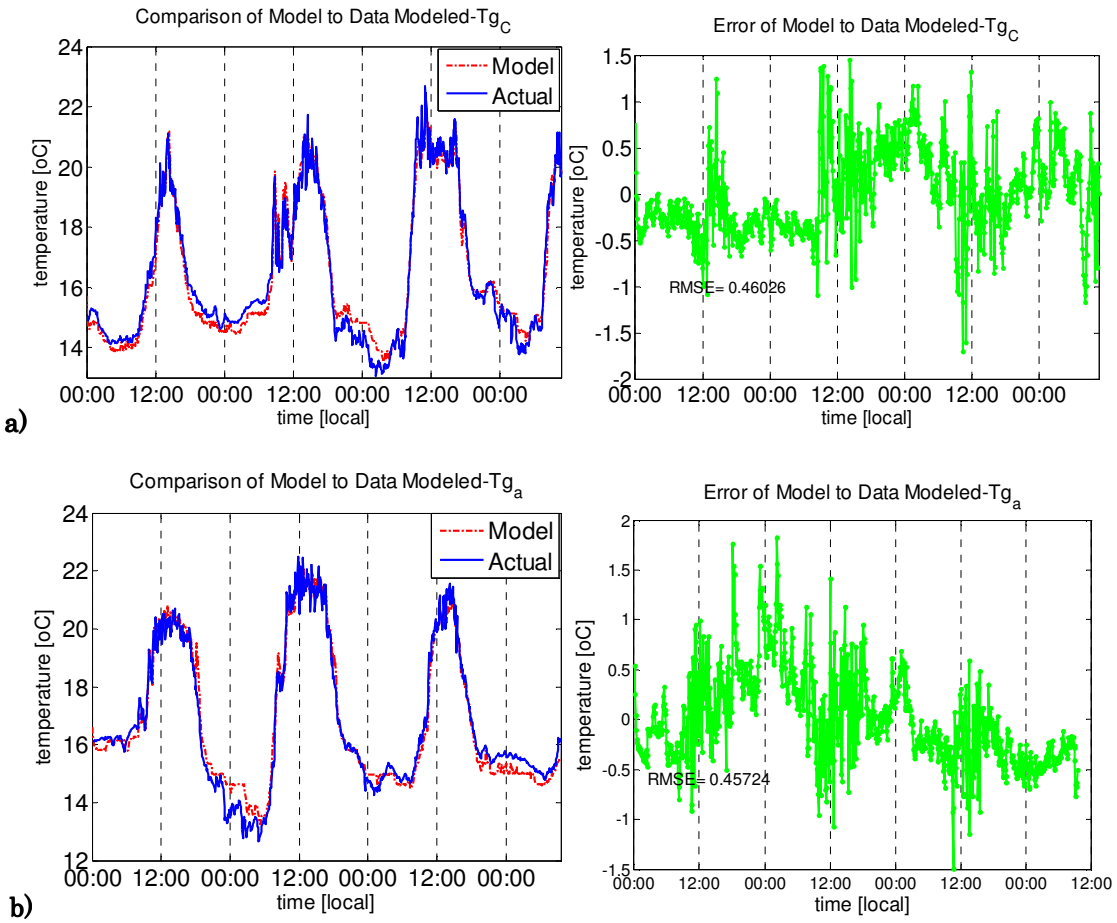

Figure 9: a) [left] Modeled temperature of offset air gap(T_{gc})compared to actual, [right] Error of model with RMS = 0.46026°C; b) [left] Modeled temperature of Angle air gap (T_{ga})compared to actual, [right] Error of model with RMSE= 0.45724°C.The subscript indicates offset (control= c and angled =a).

T_{r2}, the exposed roof temperature, was a major component in determining the inside air temperature since all the designs had two dimensional heat fluxes. This made modeling this temperature key. For all the roof models, the temperature of the roof was dependent on net radiation, convection, and conduction in the blue control volume (Figures 2, 3, and 4). Unlike the temperature of the roof under the solar panel, $T_{r2}$was the first layer exposed to the environment. Since the heat balances of equations 4, 6, and 8 were non-

linear, Newton's method of solving was chosen. Newton's method used the balance of heat fluxes and its Jacobian to estimate each iterative value.

Another significant temperature that affected the inside temperature of the building was the under panel roof temperature, which was the final temperature that was modeled. The strategy was to use the heat fluxes explained in Section 2.7 and the modeled T_{pv}, T_g, and T_{r2} to solve for T_r. Newton's method was again used in a similar fashion as the T_{r2} to model the exposed roof temperature, but now including some components that T_{r2} had removed from its heat transfer analysis.

2.5. Calibration and errors

In order to conduct accurate measurements, calibrations of all the sensors were necessary. Surface temperature was measured using YSI44016 thermistors affixed to the surfaces using thermally conductive epoxy. These thermistors used a change in resistance to measure the temperature. Air temperatures were measured using Campbell Scientific T107L temperature sensors, which were considered standard relative to the thermistors. Radiation shields covered the T107L's that were located inside the buildings in order to avoid radiative heating of the T107L when enclosed. Linear regressions (Figure 10) were estimated for the thermistors correlated to the T107L's after the sensors were tested at different temperatures.

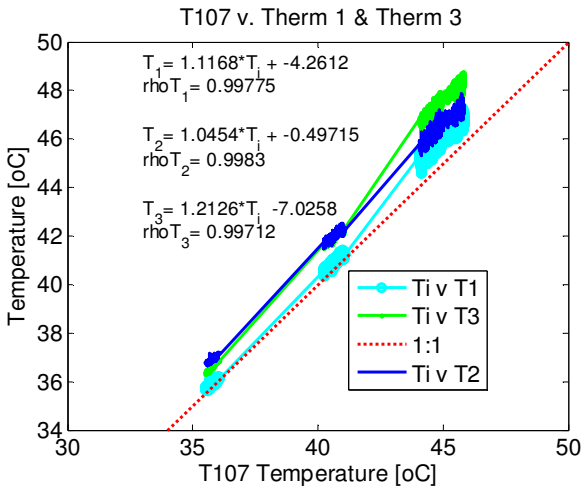

Figure 10: Example of linear regressions performed for calibrating the thermistors. Each thermistor was correlated to the T107L sensor.

Outside shortwave radiation was measured using both Kipp & Zonen and Licor 200X pyranometers. Similar linear regressions were calculated for both radiation sensors during a clear sunny day of testing, using the already established DEMROES pyranometer as the standard (Figure 11).

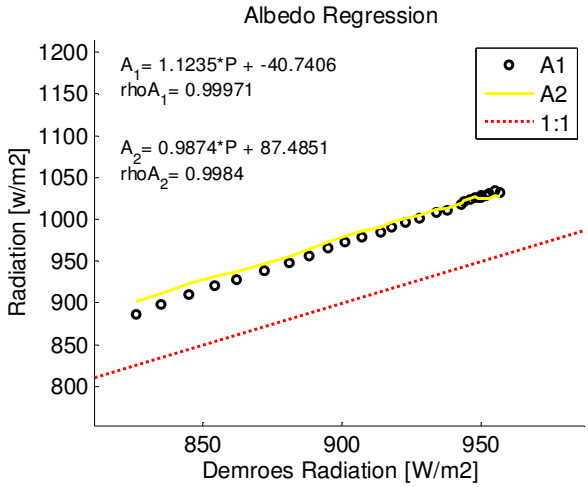

Figure 11: Linear calibration regressions for K&Z pyranometers. DEMROES pyrometer was considered standard.

3. RESULTS

This section will analyze the two different setups of the experiment and the noteworthy plots. It will also explain the seasonal modeling of the temperatures which was eventually used to estimate heat fluxes.

3.1. Setup #1

Figure 12 plots general meteorological measurements from setup #1 taken from the DEMROES weather station. The first of the three day test had the lowest wind speeds while the other two days had relatively close wind speeds.

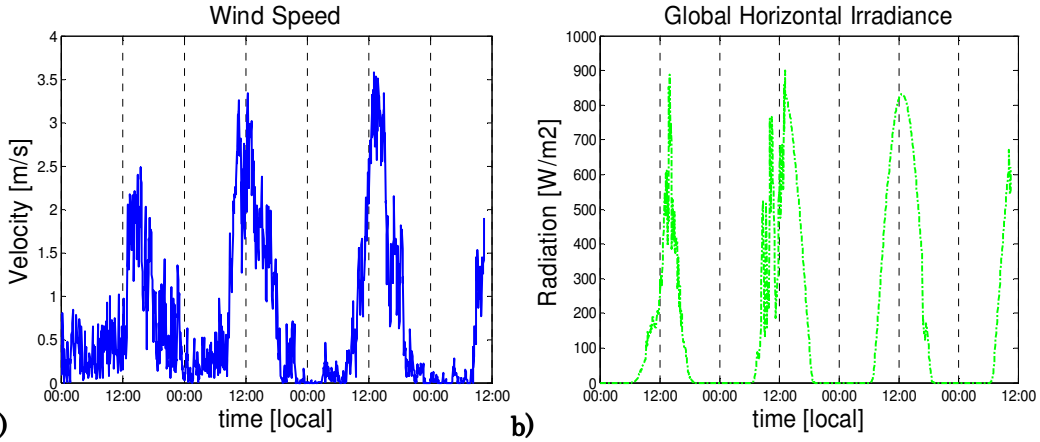

a) b)

Figure 12: a) Wind speed of the DEMROES weather station during the 3.5 day test of setup #1. b) GHI measured from the DEMROES weather station during the test of setup #1.GHI represents the amount of cloud coverage during the test.

The GHI measurements were a representation of how much cloud coverage there was during the tests. The first day experienced a mostly cloudy day with small periods of clear sky. From the curve for the second day, the units experienced morning clouds but a fairly clear day in the afternoon, which is common at UCSD. The third day had an ideal curve for a dominantly clear day with a peak around noon.

The significant temperatures of setup #1 are illustrated in Figure 13. The flush roof temperature was considerably larger, even more than the exposed roof temperature (Figure 13a), and its ceiling temperature was higher than both the roof and ceiling temperatures of the offset unit for the whole test. Also, there was a larger temperature difference between the roof and ceiling of the flush unit versus the offset unit. The outside air temperature stayed relatively constant during the 3.5 day test (Figure 13b). In both the flush and offset units, the panel's temperatures were higher than the outside air temperature during the days as expected, however, they dropped lower than air temperature during the nights. In fact, the temperatures of the flush panel during the night were less than the offset unit. Throughout the whole test, though, the temperature of the flush roof was larger than the temperature of its ceiling.

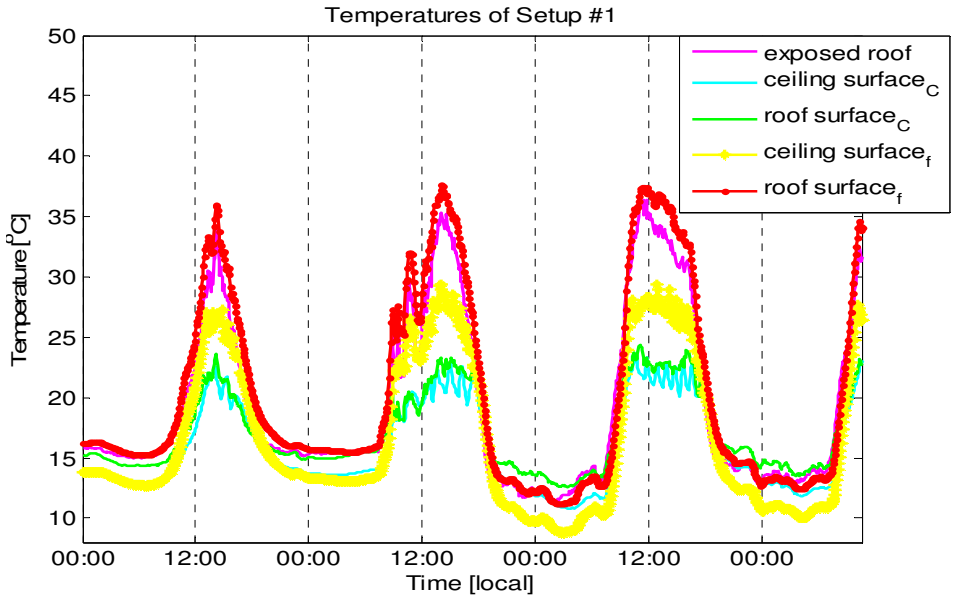

a)

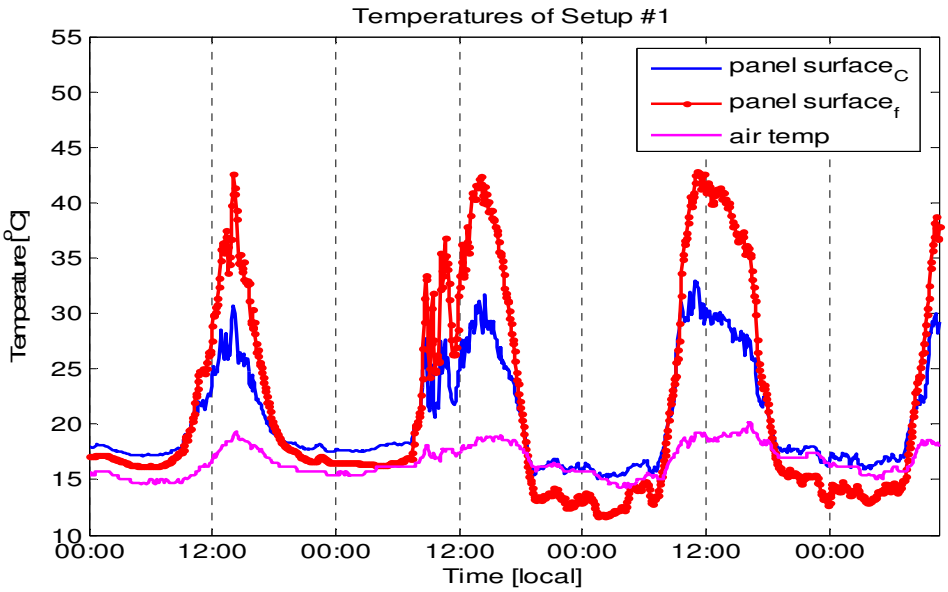

b)

Figure 13: Measured temperatures of setup #1 over 3.5 days: a) comparison of roof and ceiling temperatures; b) Comparison of air and panel temperatures. The subscript indicates offset (control = c) and flush (f).

Figure 14 shows the temperature profiles through the 32 Crank Nicholson layers for both the exposed and under panel roofs for the units. For the offset unit, under the panel temperatures were generally constant through the layers from the roof to ceiling with temperatures reaching of maximum of ~24°C, indicating that heat conduction was small. This differed from the exposed roof

since the temperature gradually decreased down the layers by ~15°C degrees during the day, indicating large heat conduction and storage.

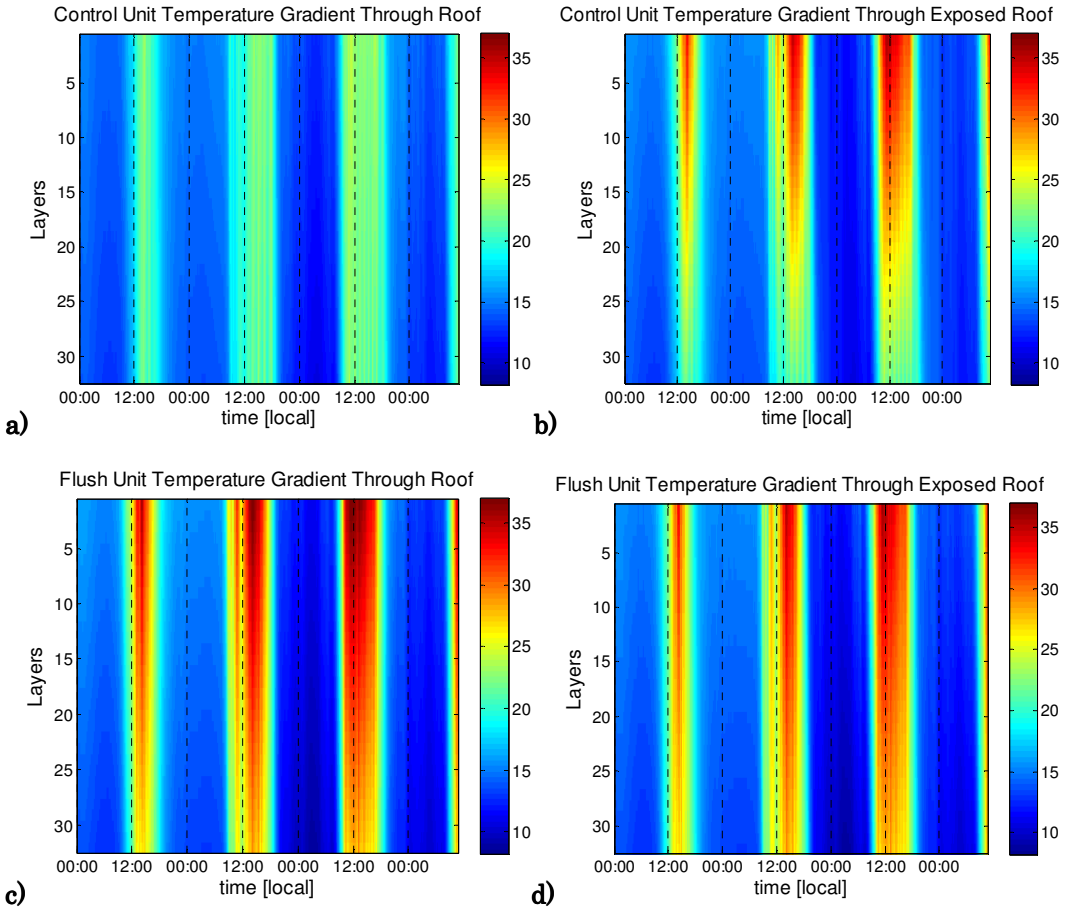

Figure 14: For setup #1 - a) & c) temperatures through the roof under the panel; b) & d) temperatures through the roof of the exposed area. Ceiling and roof surface temperature were measured and roof layer temperature were modeled using a Crank-Nicholson method.

Similar to the exposed roof area for the offset unit, both the exposed and under panel temperatures of the flush unit gradually decreased as the Crank Nicholson layers increased (Figure 14c and 14d). The temperature difference between the roof and ceiling was approximately 10°C during the day. In both under panel roofs, during the nights there were slight temperature differences where the roof temperatures were still greater than the ceiling temperatures.

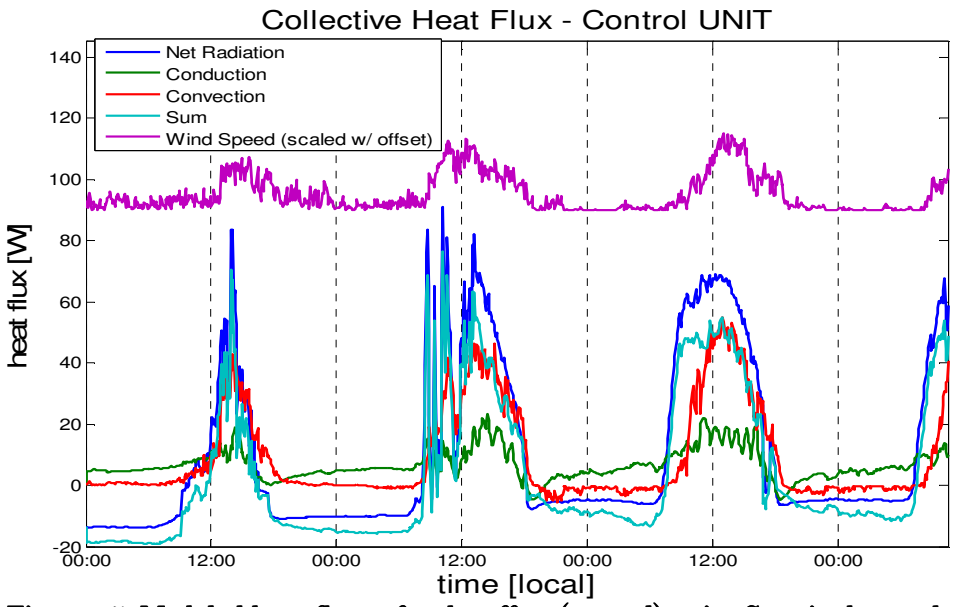

Figure 15: Modeled heat fluxes for the offset (control) unit. Sum is the conductive and radiation fluxes combined, which should be equal to the convection. The wind speed was multiplied by 7 and offset by 90.

Figures 15 and 16 shows the heat fluxes and energy balance during the entire test. Net radiation (shortwave and longwave) had the largest influence on both the systems. Although the values for radiation varied greatly between the units during the day, during the night time, they both generally decreased to similar negative values. As discussed earlier, the radiation calculations confirm that the first day was cloudy and the last day of testing there was mostly clear sky. Measurements of the radiations for the K&Z (under the panel) and LiCor 200x (adjacent to the panel) pyranometers are in Appendix F. As expected, the convection heat transfer trends were similar to that of the wind speed, which was assumed to be the same for both units. For the flush unit, the conductive heat fluxes had almost the same influence on the heat transfer as the radiation. Since the conduction through the roof was always positive (i.e. downward) for both the units, the solar panel covered roof was a heat source and kept the heat inside the units. This would be good for cold areas where it is important to reduce heat

losses and associated heating load. Detailed plots of the individual heat fluxes are also in Appendix F. In these figures, the sum referred to the net radiation and conduction, which was to equal the convection from the heat transfer balance. This was accurate during the daytime hours; however the sum is much smaller during the night.

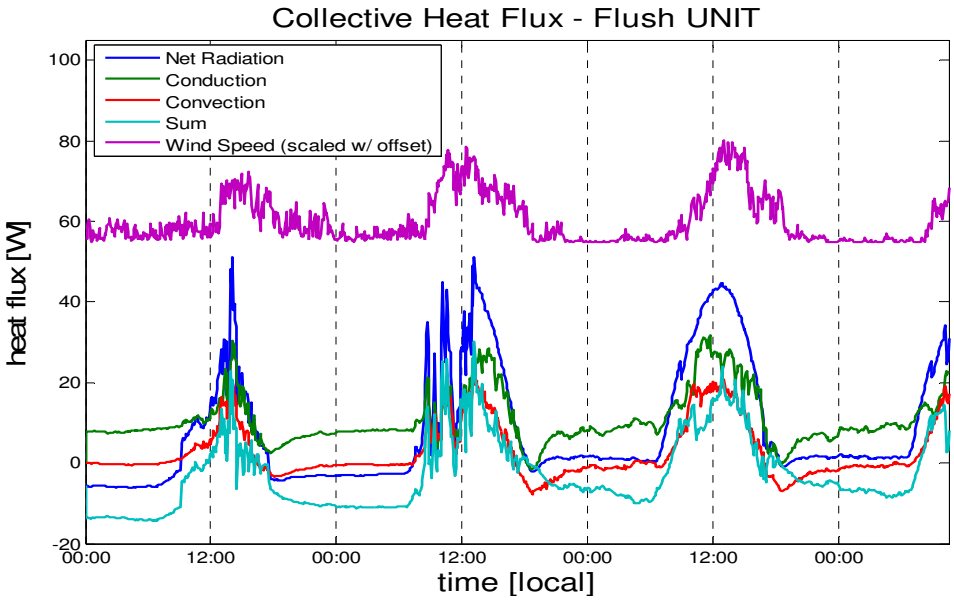

Figure 16: Collective heat fluxes for the flush unit. Sum is the conductive and radiation fluxes combined, which should be equal to the convection. The wind speed was multiplied by 7 and offset by 55.

3.2. Setup #2

Figure 19 shows the wind speed measurements from setup #2 taken from the DEMROES weather station. The first day wind speeds were the largest, with a peak at around 4 m/s which is higher than any of the wind speeds in setup #1. From there the wind speed gradually decreased from day to day. The diurnal cycles were consistent with peaks around 14:00 and small wind speeds at night.

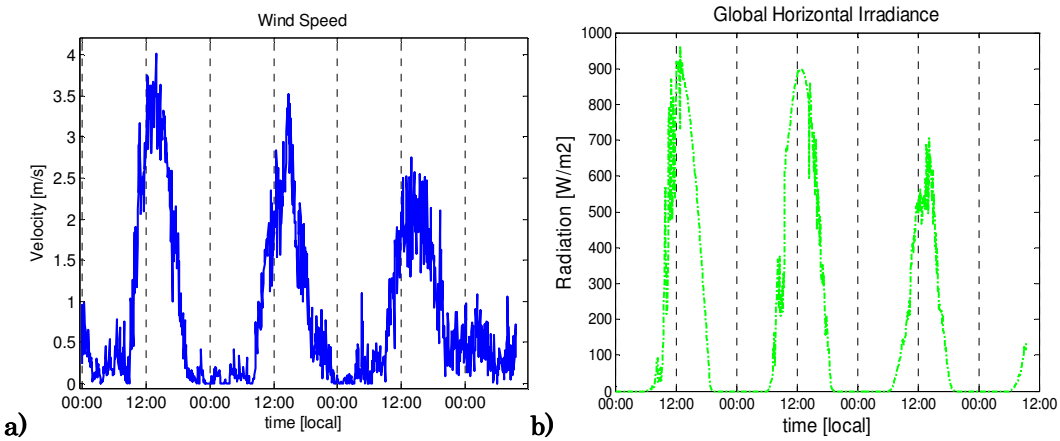

a) b)

Figure 17: a) Wind speed of the DEMROES weather station during the 3.5 day test of setup #2. b) GHI measured from the DEMROES weather station during the test. GHI represents the amount of cloud coverage during the test.

Figure 17b show the GHI measurements from the DEMROES station for the 3.5 day test of setup #2. The first day experienced morning clouds but a fairly clear day in the afternoon, similar to the second day of setup #1. For the second day of testing the clouds coverage was intermittent during the entire day, but it was still mostly sunny. The third day had the most cloud coverage, presumably overcast, with the lowest midday GHI around noon.

Temperatures for setup #2 are in Figure 18. Though the temperatures of the offset and angled units are very close during the whole test, generally the roof temperature under the angled solar panel was larger in Figure 18a. All the temperatures of the units drop below the air temperature during night, similar to setup #1. The temperature of the offset solar panel are higher than the angled panel (Figure 18b) during the day, however, they drop below the angle unit's solar panel at night time. During the entire test, the exposed roof temperature remained higher than both units' panel temperatures.

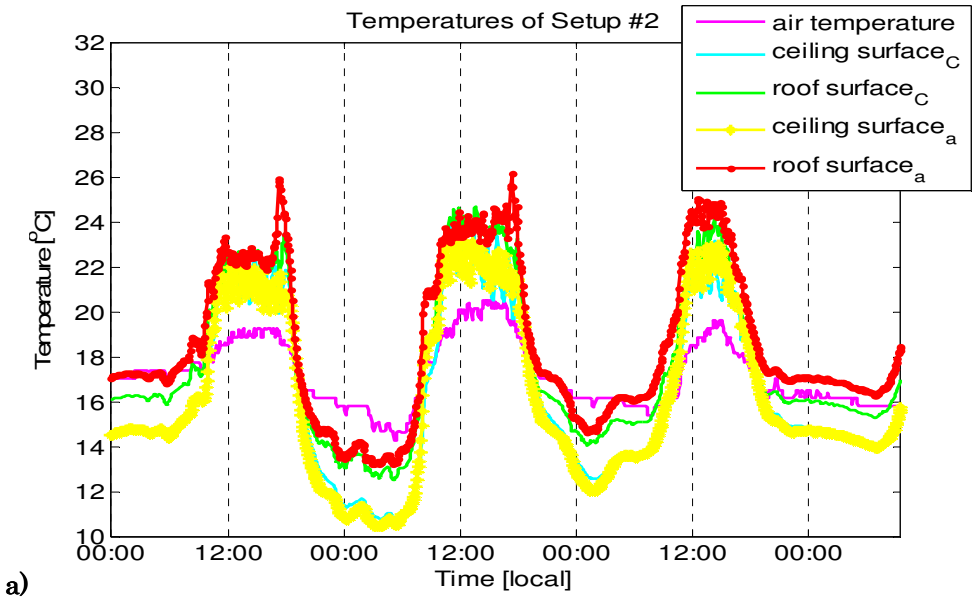

a)

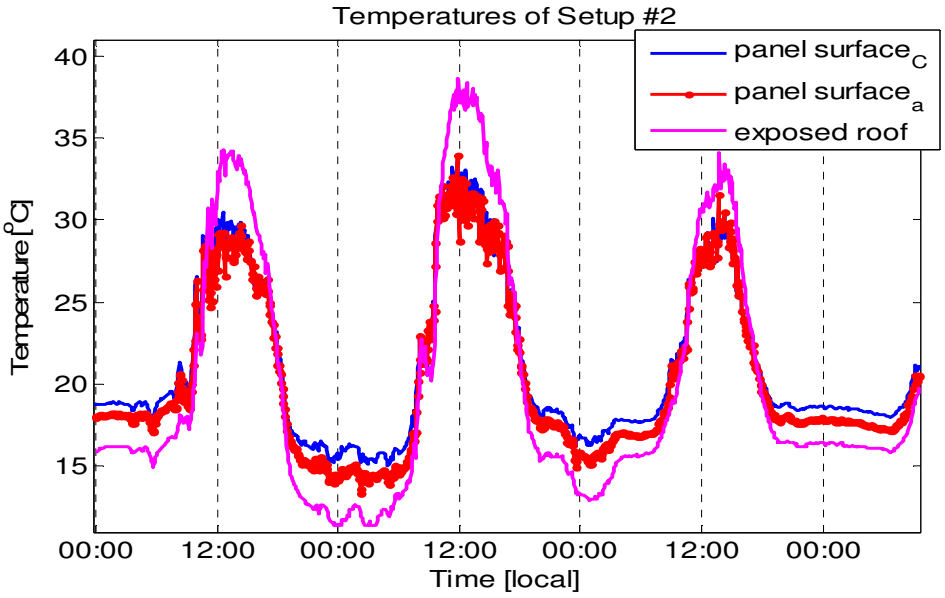

b)

Figure 18: Measured temperatures of setup #2 over 3.5 days; a) air temperature and comparison of roof and ceiling temperatures; b) exposed roof and comparison of panel temperatures. The subscript indicates offset (control = c) and flush (f).

For the temperature profile through the layers of the roof (Figure 19), the offset unit experienced similar trends as setup #1. The under panel roof temperature of the angled unit had a gradual decreasing temperature of approximately 4°C in difference as the layers increased from the roof to the ceiling during the day time.

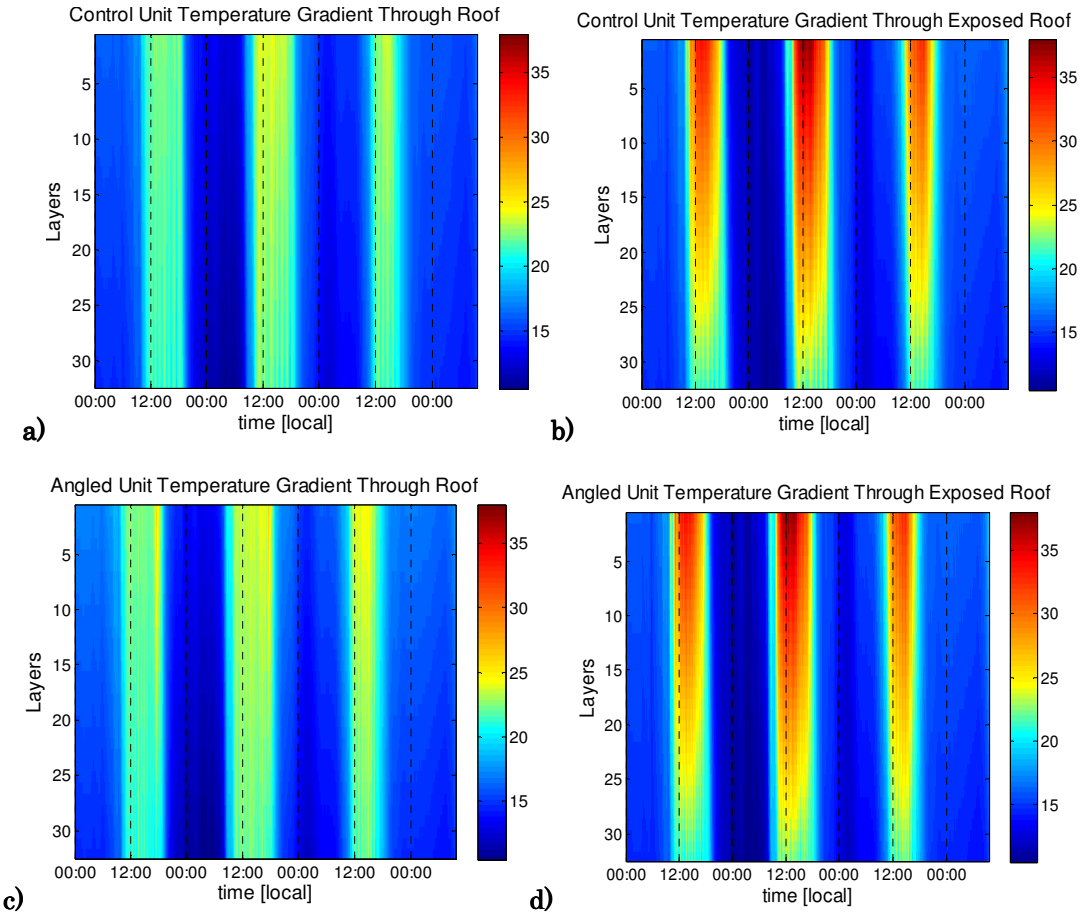

Figure 19: For setup #2 - a) & c) temperatures through the roof under the panel; b) & d) temperatures through the roof of the exposed area. Ceiling and roof surface temperature were measured and roof layer temperature were modeled using a Crank-Nicholson method.

The temperature profile of the exposed area of the angled unit was almost identical to the offset units' exposed area. The temperature difference during the day time was approximately 15°C, similar to setup #1. Also, the roof temperature was greater than the ceiling temperature during the entire test, even at night time.

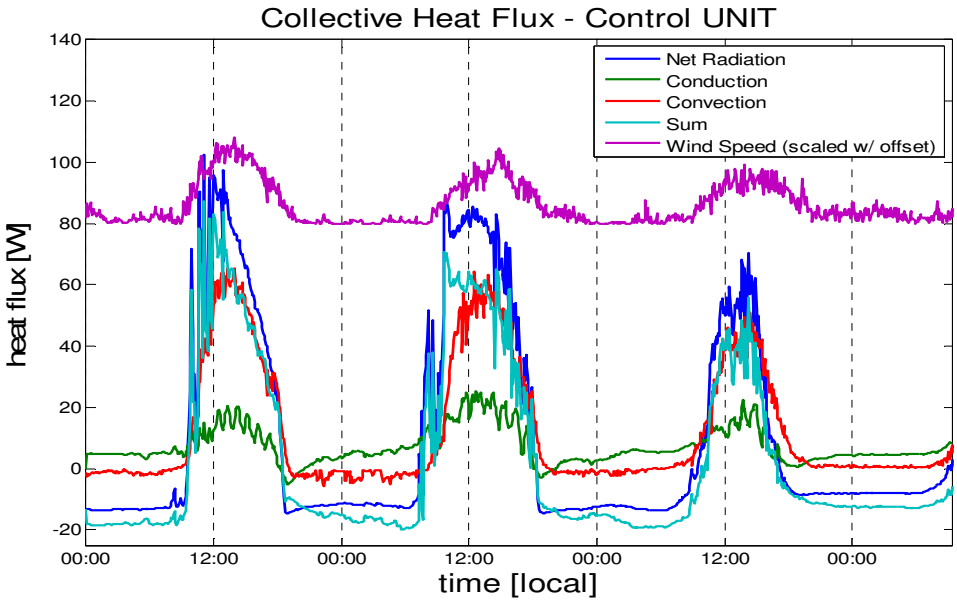

Figure 20: Collective heat fluxes for the offset unit during setup #2 test. Sum is the conductive and radiation fluxes combined, which should be equal to the convection. The wind speed was multiplied by 7 and offset by 80.

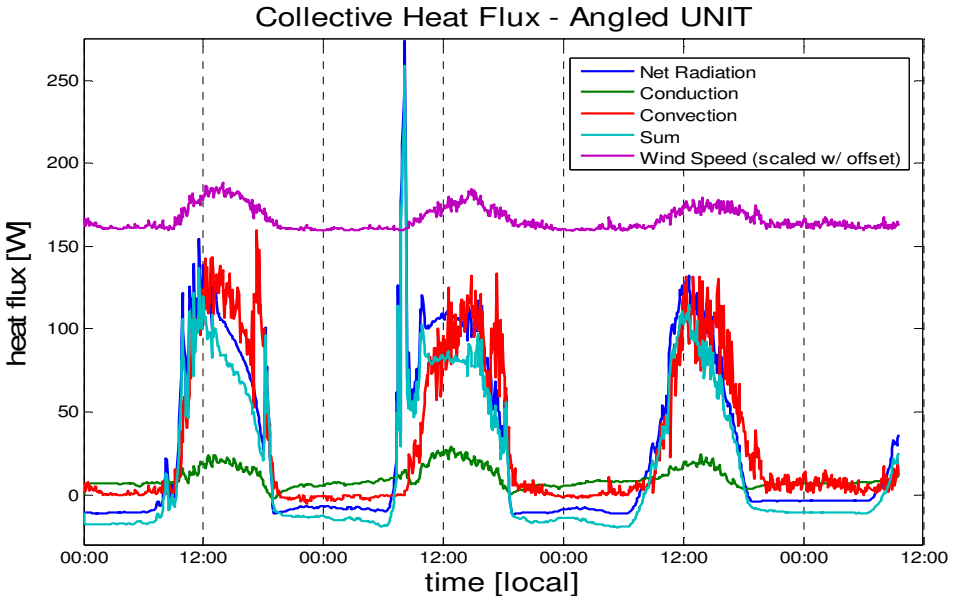

Figure 21: Collective heat fluxes for the angled unit during setup #2 test. Sum is the conductive and radiation fluxes combined, which should be equal to the convection. The wind speed was multiplied by 7 and offset by 160.

The energy balances for setup #2 are in Figures 20 and 21. For the offset unit, it was apparent that net radiation still played the largest role in the heat transfer. For the angled unit, the convective heat flux also played a big part in

the heat balance since it was almost as large as the net radiation during most of test. At the peaks of all three days, the convective flux was even more influential than any of the other heat fluxes. For both units at night time, although the convection heat flux dropped, it was not as much as the net radiation, which was a similar trend as setup #1. The angled unit experienced a large spike of shortwave radiation underneath the solar panel during the second day (Appendix G), which was observed in the net radiation. These values of radiation were larger than atmospheric GHI, which leads to the discussion of how the sensor measured this value. A possible explanation is the sensor under the panel may have received shortwave radiation from the solar panel in addition to the sun. On that day, at those certain times, the sun may have been at such an angle that it was reflecting underneath the solar panel and onto the sensor. These large shortwave radiation values were not considered during the calculations of the models.

3.3. Cooling Load Comparison

Table 3 shows the hourly details of the frequency of HVAC usage during setup #1 (Plots are in Appendix J). The HVAC system was used least on the first day of setup #1 for both units. From Figure 12, although the wind speeds were relatively smaller, that day was the cloudiest of the entire test. For the first day, the flush unit started the HVAC system around the same time as the offset unit, but continued on after the offset unit turned off. For the flush unit on the other two days of setup #1, the HVAC system started earlier in the day, around 11:00, and continued longer into the afternoon. On the second day, the flush unit started and finished earlier than the offset, whereas during the third day the

flush unit operating hours were consistent with the offset. On the third day, the HVAC systems for the units were running the longest, and hence the energy usage was the largest during this day. Although the offset and flush units had similar trends, Table 3 also shows that ultimately the energy usage in the flush unit was always higher than the offset unit.

Table 3: Average power draw (work) of the HVAC system for the offset (control) and flush units during first 3 days of Setup #1. Totals on the bottom represent the total HVAC energy usage for that day. Other times of the day are not presented since the HVAC did not turn on.

	Day 1		Day 2			Day 3		
Hour [hh:mm]	**Offset [W]**	**Flush [W]**	**Hour [hh:mm]**	**Offset [W]**	**Flush [W]**	**Hour [hh:mm]**	**Offset [W]**	**Flush [W]**
11:00	0	0	11:00	0	85	11:00	83	249
12:00	0	0	12:00	0	56	12:00	272	327
13:00	0	0	13:00	56	169	13:00	222	304
14:00	0	251	14:00	195	251	14:00	221	331
15:00	247	301	15:00	221	334	15:00	219	274
16:00	139	194	16:00	304	303	16:00	218	299
17:00	0	140	17:00	195	249	17:00	243	270
18:00	0	0	18:00	56	83	18:00	27	111
19:00	0	0	19:00	56	0	19:00	0	0
Total [Wh]	**386**	**887**	**Total [Wh]**	**1083**	**1530**	**Total [Wh]**	**1505**	**2165**

Table 4: Average power draw (work) of the HVAC system for the offset (control) and angled units during first 3 days of Setup #2. Totals on the bottom represent the total HVAC energy usage for that day. Other times of the day are not presented since the HVAC did not turn on.

	Day 1			Day 2			Day 3	
Hour [hh:mm]	**Offset [W]**	**Angled [W]**	**Hour [hh:mm]**	**Offset [W]**	**Angled [W]**	**Hour [hh:mm]**	**Offset [W]**	**Angled [W]**
12:00	0	120	12:00	296	296	12:00	0	60
13:00	180	180	13:00	324	324	13:00	209	300
14:00	209	238	14:00	293	293	14:00	238	208
15:00	209	209	15:00	233	233	15:00	267	325
16:00	178	178	16:00	233	233	16:00	238	209
17:00	119	208	17:00	205	205	17:00	61	121
18:00	149	120	18:00	177	177	18:00	30	30
Total [Wh]	**655**	**953**	**Total [Wh]**	**1464**	**1761**	**Total [Wh]**	**1044**	**1254**

Table 4 shows the diurnal cycle of HVAC usage during setup #2 (plots are in Appendix J). The offset and angled units HVAC system operated mostly synchronously. With a closer look into all 3.5 days (Figure 60 in Appendix J), the angled unit started the HVAC slightly earlier during the day and turned off slightly later. The energy usage of the offset unit was again less than the angled unit for all three days of the test, with the least energy used on the first day. The HVAC usage compared to the temperatures for both setups can be found in Appendix F and G.

Table 5: Total energy usage by HVACs for both setups in Wh.

Setup #	Offset	Flush/ Angled	% difference
1	238Wh	380Wh	60
2	308Wh	358Wh	16

Table 5 is a comparison of the heat extracted by the HVAC for all the units during its entire test. Based on the high temperatures measured on and in the flush unit (panel down to the ceiling) it could be expected that it would have the largest heat extracted. From setup #2, the angled unit also had higher energy

usage than the offset to maintain the inside temperature, though the difference between the offset and flush is much larger than the offset and angled unit.

3.4. Seasonal Modeling

3.4.1. Modeling- Exposed Roof

Figures 22, 23 and 24 are the modeled exposed roof temperatures for the offset, flush and angled units respectively. The modeled temperatures were then compared to the measured temperatures. Note that the test and 'training' datasets were not independent, so the results may be less accurate for other times. The modeled gap and panel temperatures are part of the inputs into the exposed roof model.

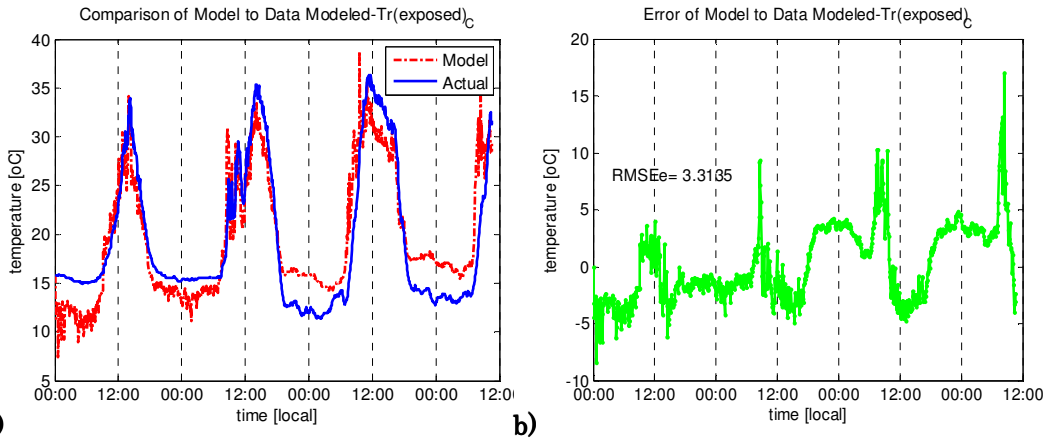

a) b)

Figure 22: a) Modeled temperature of exposed roof $T_{r2,c}$ compared to actual for offset unit, b) error of model with RMSE= 3.3135°C.

From Figure 22b, with a root mean square error (RMSE) of 3.31°C, the exposed roof model for the offset unit seemed to be closer to the actual temperatures during the daytime hours; however there was a great discrepancy during night time. However, even during the day time, the model tended to underestimate the peak temperatures.

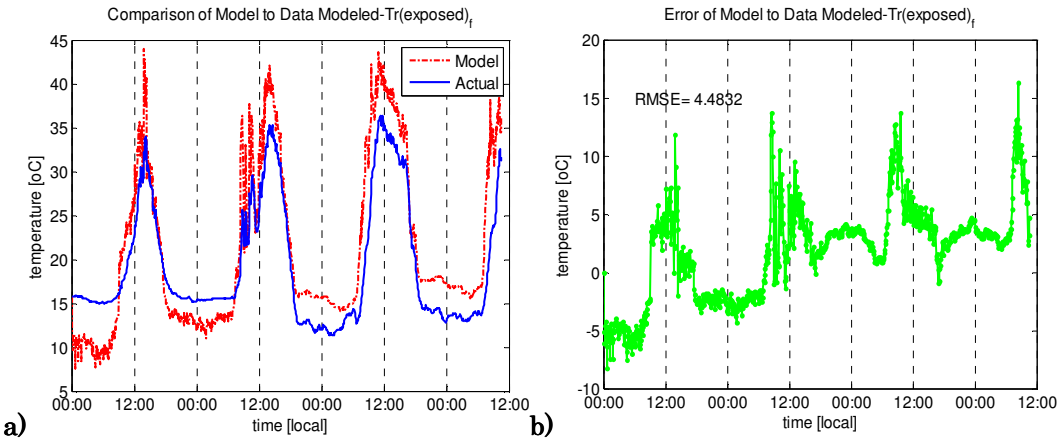

a) b)

Figure 23: a) Modeled temperature of exposed roof $T_{r2,f}$ compared to actual for Flush unit, b) error of model with RMSE= 4.4832°C.

Unlike the offset unit, the modeled flush temperatures seemed to have generally the same error during the day time and the night time, with an RMSE of 4.5°C (Figure 23b). The modeled values were overestimated during the peak daytime temperatures compared to actual, while the over or under estimation varied during the night time depending on the day.

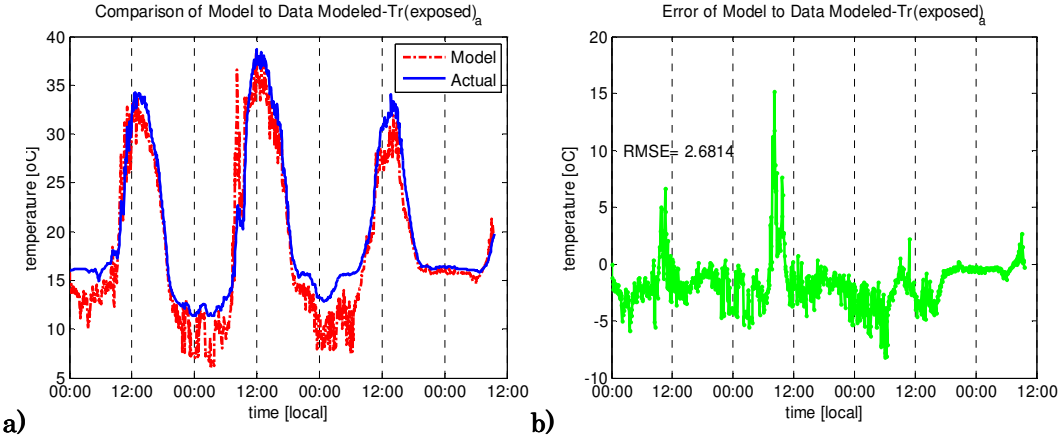

a) b)

Figure 24: a) Modeled temperature of exposed roof $T_{r2,a}$ compared to actual for Angled unit, b) error of model with RMSE= 2.6314°C.

Of all the exposed modeled temperatures, the angled unit was the closest to the actual, with a RMSE of 2.63°C (Figure 24b). The exposed roof model seemed to be closer to the actual temperatures during the daytime hours, with a

fluctuation of discrepancy during night time. Similar to the offset unit, the model tended to underestimate the peak temperatures during the day. The model for the exposed roof of the offset unit was also relatively close to the actual temperatures especially during the day when the modeling was significant although its error was slightly larger than the angled unit.

For all three of the models, regardless of the amount of error, the shapes of the plots were approximately the same as the actual. The priority of the models were the day time temperature accuracy since the heat flux during that time would be larger, and inside the units would therefore experience higher temperatures. For this reason, although the night time models had a larger error than the day time, this was not considered crucial.

3.4.2. Modeling –Back Panel

Figures 25, 26, and 27 show the modeled temperatures of the roofs under the solar panels as well as their errors. These temperatures were modeled using the modeled T_g, T_{pv}, and T_{r2} as inputs. For the offset unit's model, the error seemed to be equal between the day and night times, with a RMSE of 4.73°C. As was seen in earlier models, the modeled temperatures were higher than the actual during the day time, particularly during midday, and lower than actual during the night.

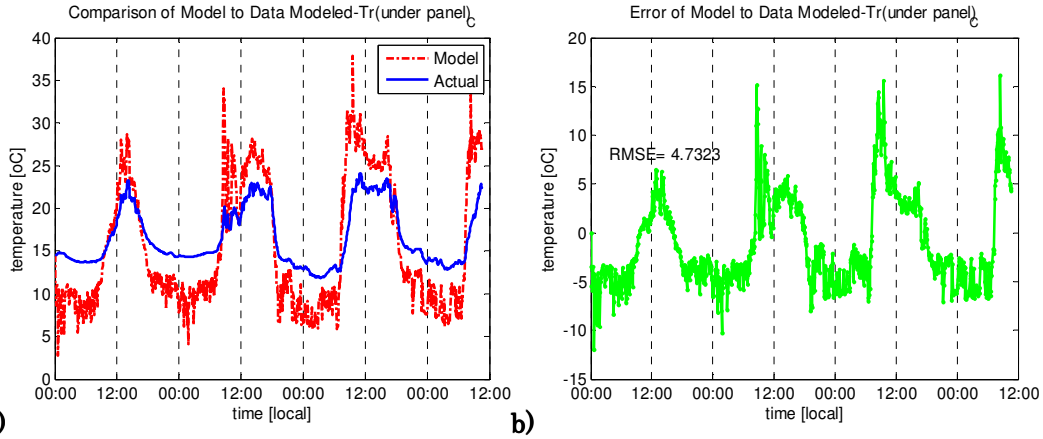

a) b)

Figure 25: a) Modeled temperature of roof under the solar panel $T_{r,c}$compared to actual for offset unit, b) error of model with RMSE= 4.7323°C.

The flush unit's modeled back panel temperatures overestimated during the day and underestimates during the night time as well. The error during the day time was larger than the night time. The RMSE of the flush unit was 4.72°C (Figure 26b). Like the exposed area temperature models, the shapes of the modeled flush unit's under panel temperature were also very similar to the actual. The flush temperature models for both the exposed and back panel temperatures had generally a larger error than that of the offset and angled units. The reason could be that the heat transfer on the flush unit was not 1-

dimensional with horizontal heat transfer occurring between the exposed roof and shaded part of the roof. During the validation of the heat transfer dimensions from Appendix B, the flush solar panel could not be tested because there was trouble in sealing the large panel to the roof with caulk as was done with the smaller panel.

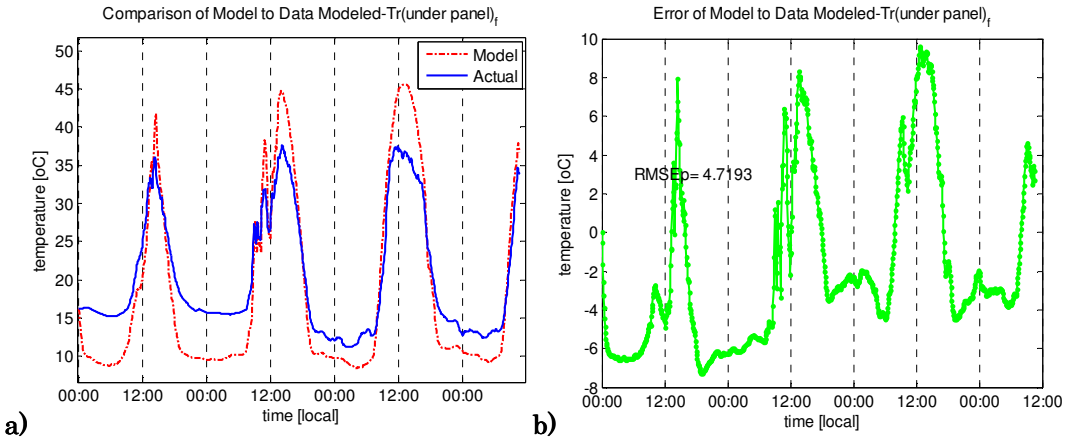

a) b)

Figure 26: a) Modeled temperature of roof under the solar panel $T_{r,f}$ compared to actual for flush unit, b) error of model with RMSE= 4.7193°C.

The error of the back panel temperatures for the angled unit was the least then the other designs, at RMSE approximately 1.99°C (Figure 27b). However, the difference between the modeled temperature and the actual during the peak hours of the day was about 4°C, which is greater than the other models. As was the case for the flush and offset units, the modeled temperatures for the under the angled panel were overestimated temperatures during the day time and underestimated some of the nights.

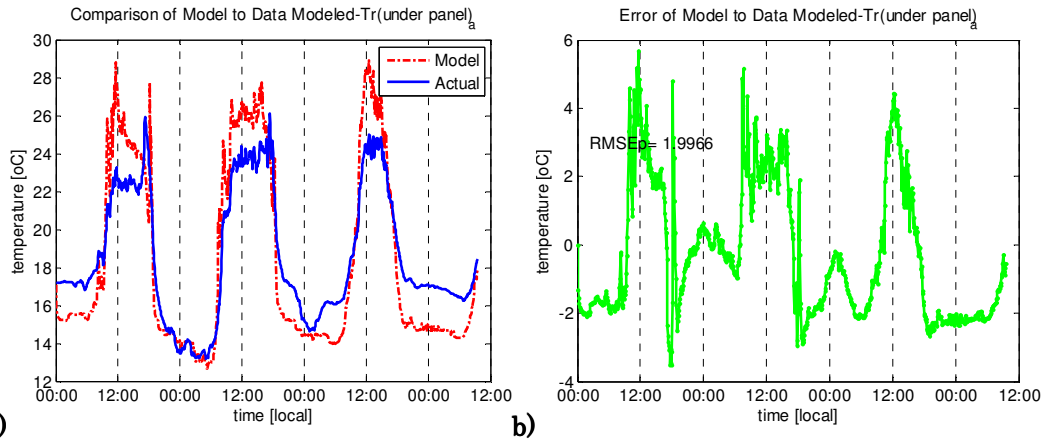

a) b)

Figure 27: a) Modeled temperature of roof under the solar panel $T_{r,a}$ compared to actual, b) error of model with RMSE= 1.9968°C.

All three cases had large errors in the models for the back panel temperature. For the back panel modeled temperatures of the offset unit, the error during midday was large. When the original values for the T_{pv}, T_{r2} and T_g, were used instead, the models became more accurate to the actual back panel temperatures (Appendix I).

3.4.3. Summer Heat Flux

With forcing data from the continuously operating DEMROES station, the heat transfer models described in sections 3.4.1 and 3.4.2, and the assumption that T_s (ceiling temperature) was linearly related to the temperatures of the roof, heat flux through the roof for different times of the year was calculated. Table 6 shows the heat flux from conduction for twelve weeks of the 2010 summer at UCSD RIMAC using the modeled temperatures for all three solar panel designs. The heat flux varied with the meteorological conditions during the summer. The week of July 4, 2010 had the least amount of heat flux for all three designs. Overall, the sum of the heat flux for the flush solar panel was the most, offset

solar panel was second with 29% less conduction than the flush unit, and angled solar panel had the least with 43% less conduction than flush.

Table 6: Conduction heat flux through roof of units with the modeled temperatures of the different designs. The heat flux models were forced by the DEMROES stations weather measurements during summer 2010. Average air temperature and GHI are also presented.

Week of	Offset [W]	Flush [W]	Angled [W]	Avg Tair [°C]	Avg GHI [W/m²]
20-Jun-2010	2424	4923	1711	16.2	288.8
27-Jun-2010	1418	3725	1073	16.4	187.2
4-Jul-2010	503	2694	505	16.1	120.3
11-Jul-2010	5212	4874	4440	19.3	286.8
18-Jul-2010	2468	3620	2132	17.7	182.4
25-Jul-2010	2095	3632	1721	17.3	177.1
1-Aug-2010	3324	4784	2440	17.7	265.8
8-Aug-2010	3207	4694	2468	17.5	262.9
15-Aug-2010	4898	4716	4056	19.4	265.3
22-Aug-2010	5016	4706	4224	19.7	261.2
29-Aug-2010	3085	4544	2312	17.7	243.7
5-Sep-2010	2309	3918	1868	17.4	196.4
Total [kWh]	**6.0**	**8.5**	**4.9**		

4. DISCUSSION AND CONCLUSIONS

There are many inferences that can be made about the photovoltaic roof heat flux of the solar panel designs used in this project. Designating the offset unit as the control created an opportunity to observe the significance of each heat transfer in the control volumes with relation to the solar panel height and tilt. The heat fluxes through the roof of the angled unit were the highest, with the largest fluxes ranging from approximately 100-150 W (not including the spikes on the second day). From setup #2, the angled heat fluxes were almost 20% higher than the offset unit's heat fluxes. Setup #1 showed that the offset unit heat fluxes were 60% greater than the flush unit. While the largest values of the heat transfer 'sum' in the offset unit (Figure 15) ranged from 50-80 W, the flush unit heat fluxes barely reached 20 W (Figure 16). From Table 5, the heat extracted in the offset unit to maintain 21.5°C was the smallest, i.e. the temperatures inside the offset were less than both the angled and flush. Consequently, less work from the HVAC system was required for the offset indicating a reduction in cooling loads and energy use.

Following the offset design, the next solar panel design that minimized HVAC usage was the angled unit. From the heat transfer analysis of setup #2, the angled and offset units were very close in temperatures, and Table 5 was necessary to show which setup had a smaller cooling load overall. Relative to the other two designs, the angled design had more exposure to the environment due to the tilt in the solar panel. Although there was more convection in the angled unit than for the offset unit, this upward heat flux could not overcome the

downward fluxes from radiation (longwave and shortwave) which made the temperatures inside greater than the temperatures inside the offset unit. This proved that for these solar panel designs, radiation had the greatest influence on the temperatures inside the building.

Finally, the flush unit had the largest cooling load. Figure 13a showed that the temperature of the exposed roof was almost the same as under the panel roof, which meant that the solar panel did not cause any reduction in roof temperature, and as a consequence in roof heat flux. The 60% increase in heat extraction from the flush unit versus the offset unit was significant. The main distinction between the flush unit and the other two units was the mode of convection at the back panel: natural convection for the flush unit and forced convection for the other units. Installing a solar panel with the 0.076m offset did introduce shortwave radiation to the roof; however, in this case the convection heat flux was able to overcome the heat flux from the radiation. Since the forced convection depended on the wind speed, the results of this project would vary in locations with different wind speeds. For example, if the tests were conducted in an area with relatively low wind speeds, the forced convection influence would be less in the overall heat transfer through the roof.

The heat balance figures (Figures 15, 16, 20, and 21) showed that the convective heat transfer coefficients discussed in Section 2.3.3 for the exposed and under panel roof area off all three units were in good agreement. For the heat transfer analysis, the difference of net radiation and conduction for the first layer of each unit's control volume was close to the total convection, indicating that the heat transfer processes were modeled with reasonable accuracy.

The main purpose of this research project was to improve solar array design from a heat transfer perspective and to initiate more of these types of tests to find the optimum design of the solar panel on a roof top. In addition to cooling loads, another factor to consider for this objective was the energy output from the actual solar panel. Since the flush and offset were not tilted, their results were the same. Utilizing PVWatts (Appendix K), the flush solar panel produced 35% of the energy specified in Table 5 for the HVAC system, while the offset unit produced 56% for Setup #1 and 43% for Setup #2. With the PVWatts calculation for the angled solar panel, 41% was saved from the energy required from Table 5 for Setup #2. From an economic point of view, SDG&E charges consumers 17.4¢/ kWh for a baseline allowance during the summer season [12]. Taking into account the remaining energy required after the solar panel input, Table 7 shows the cost to run the HVAC for an average building (1:800 ratio) based off solar panel design. The flush unit energy use was assumed to be approximately the same as a roof with no solar panel since the temperatures were relatively close. From Table 7, the offset unit saved as much as $38 compared to a roof with no solar panel during the 3.5 days of testing. As mentioned before, the solar panel had a 1:4 area ratio with the roof and expressing this value in terms of the area ratio allows for scaling to other buildings of different size. Using the area ratio, this makes the offset savings 4x $38/(panel: roof area). At this rate, from Setup #2 the angled unit had a 4x $4/(panel: roof area) difference than the offset. Since ultimately a resident is looking for energy savings and, in turn, cost effectiveness, from this project a solar panel at an offset of 0.076m and tilt of 0° is the optimal design.

Table 7: Total energy charges for the different solar panel designs for both Setup #1 and Setup #2.The calculations are based on the 1:800 ratio of the units to an average building. Rates are based off SDG&E's 17.4¢/kWh for summer seasons.

Setup #1

Panel Design	Cost
No Panel	$53.00
Flush Panel	$34.00
Offset Panel	$15.00

Setup #2

Panel Design	Cost
Offset Panel	$25.00
Angled Panel	$29.00

Examples to further the study of the solar panel design that would be beneficial are tests between the offset and different angled designs. These tests could show at which angle the heat extracted from the solar panel could be the same as the control (offset) while also calculating the energy input from the solar panel. A model could also be developed that would estimate the heat extraction as a function of the angle tilt. The results of these tests may even show an angled design that uses less heat extraction than the offset with better solar panel energy efficiency.

The other objective of this research project was to develop models of solar panel effects on a building to incorporate into building energy simulation programs such as EnergyPro. When comparing the offset and angled model to the actual temperatures of the exposed roof during the day time, the results were satisfactory. The equations used in the Newton's method for modeling the roof temperature under the PV panel were most accurate with the actual temperatures for the angled unit, especially during the day time. Presumably the reason the error for the roof under the back panel of all the units was the greatest was that the models were dependent on other modeled temperatures (recall: T_{pv}, T_{r2} and T_g, for angled and offset). The errors in those models propagated. This can also be seen from Table 6 where the offset had more heat flux through its roof

than the angled unit, which was not expected from the analysis of Table 5. Regardless, it is obvious that more data collection in different seasons would improve the models. To improve the model of the flush temperatures, further tests of the flush solar panel in 1-dimensional heat transfer could be conducted thoroughly before moving to 2-dimensions. This way there may be a scheme of finding the effects of the two roof temperatures upon each other.

BIBLIOGRAPHY

1. H Akbari, DM Kurn, SE Bretz, JW Hanford, Peak power and cooling energy savings of shade trees, *Energy and Buildings 25* (1997) 139-148.

2. ASHRAE, *Handbook of Fundamentals* (1993).

3. D. Bigot, F Miranville, AH Fakra, H Boyer, A nodal thermal model for photovoltaic systems: Impact on building temperature fields and elements of validation for tropical and humid climate conditions, *Energy and Buildings 41* (2009) 1117-1126.

4. California Public Utilities Commission, *Renewables Portfolio Standard Quarterly Report* (2008).

5. CIMIS evapotranspiration model, http://wwwcimis.water.ca.gov/cimis/infoEtoPmEquation.jsp, accessed September 25, 2010.

6. A. Dominguez, J. Kleissl, and J. Luvall. Effects of Solar Photovoltaic Panels on Roof Heat Transfer, University of California, San Diego (Unpublished).

7. G Gan, Numerical determination of adequate air gaps for building-integrated photovoltaics, *Solar Energy 83* (2009) 1253-1273.

8. AD Jones and CP Underwood, A thermal model for photovoltaic systems, *Solar Energy*, Vol. 70:4 (2001) 349 -359.

9. M Kacira, M Simsek, Yunus Babur, Sedat Demirkol, Determining optimum tilt angles and orientations of photovoltaic panels in Sanliurfa, Turkey, *Renewable Energy 29* (2004) 1265-1275.

10. T Otto, *Comparative Study of Grid Connected Photovoltaic Arrays*, Master of Sciences in Physics, San Diego State University (2009).

11. Pacific Gas &Electric, *Go Solar California: A consumer's guide to the California Solar Initiative* (2008).

12. San Diego Gas & Electric, *Energy Charge Breakdown*, http://www.sdge.com/customer/rates/rateBreakDown.shtml (2010).

13. EM Sparrow, JW Ramsey, and EA Mass, *Effect of Finite Width on Heat Transfer and Fluid Flow about an Inclined Rectangular Plate*, Journal of Heat Transfer 101 (1979) 199-204.

14. TECA, *Thermoelectric Cold Plate*, www.TECA-USA.com (2010).

15. U.S. Department of Energy, *Energy Efficiency Trends in Residential and Commercial Buildings* (2008).

16. GN Walton, *Passive Solar Extension of the Building Loads Analysis and System Thermodynamics (BLAST) Program*, United States Army Construction Engineering Research, (1981) Technical Report, Champain, IL.

17. GN Walton, *Thermal Analysis Research Program Reference Manual*, National Bureau of Standards, NBSSIR (1983) 83-2655.

18. W Tianet. al, Effect of building integrated photovoltaics on microclimate of urban canopy layer, *Building and Environment 42* (2007) 1891-1901.

19. Y Wang et. al, Influence of a building's integrated-photovoltaics on heating and cooling loads, *Applied Energy 84* (2006) 983-1003.

APPENDIX

A. HVAC unit

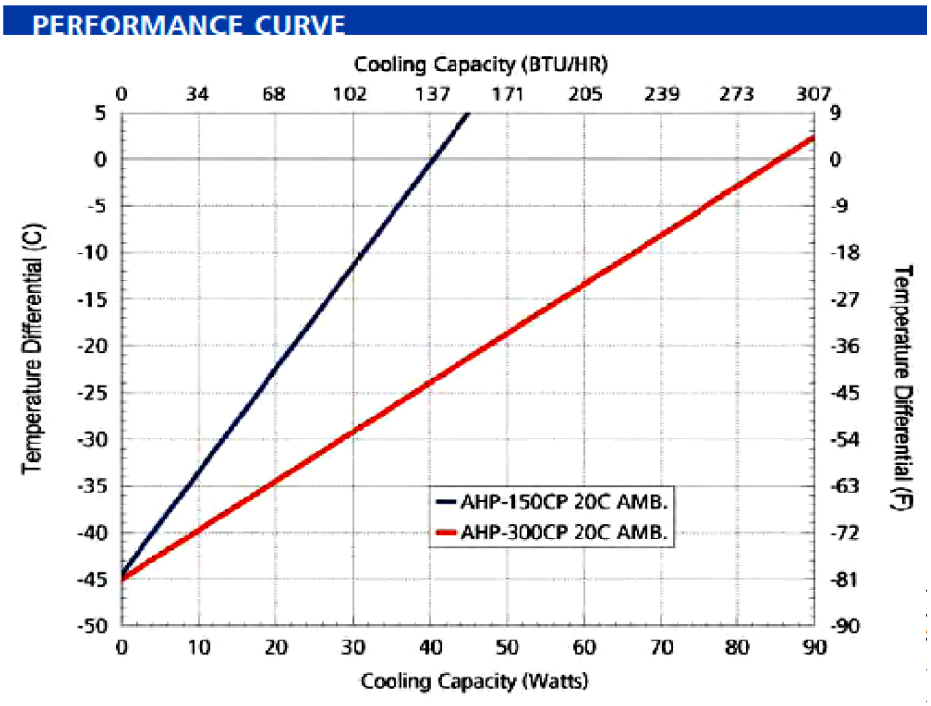

Figure 28: Performance curve of the HVAC unit- TECA 150-HP CP

B. 1D vs. 2D heat transfer validation

One major assumption that was made during both setups was that the heat flux underneath the solar panel was independent of the heat flux of the exposed area. To validate this, separate tests were conducted which compared a 1-dimensional heat flux, meaning the solar panel covering the entire roof, versus the current 2-dimensional (Figure 29). These tests were a comparison of the offset design and the angled design.

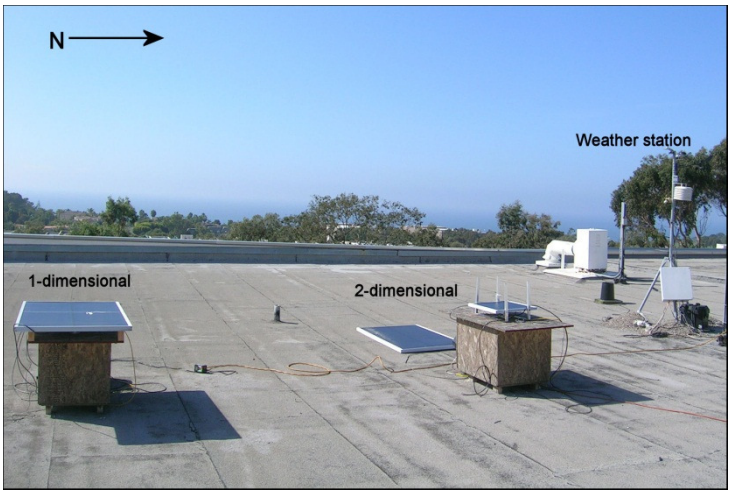

Figure 29: A photo of the setup to compare the 1-dimensional heat flux and 2-dimensional heat flux under the solar panel for the offset design.

Figure 30 shows that after the heat fluxes under the solar panels were normalized and multiplied by area ratio, they become close in value.

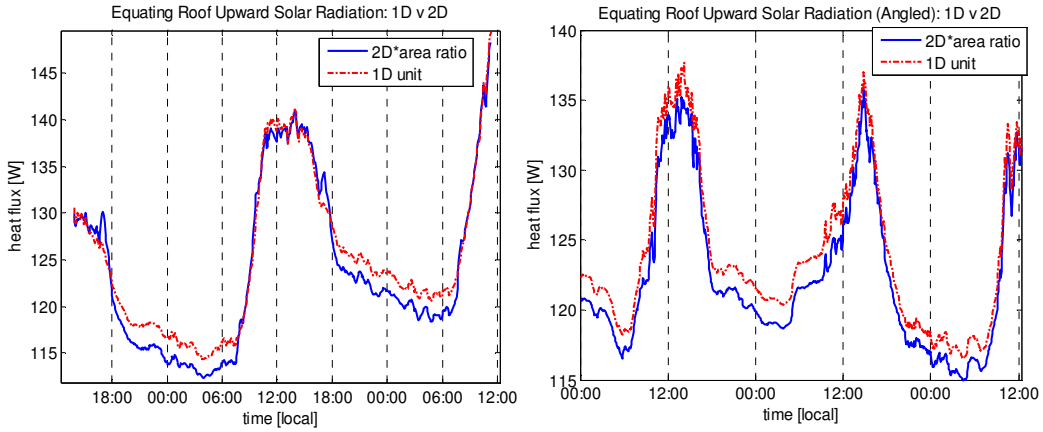

Figure 30: Normalized upward longwave radiation heat flux from roof for the 1D and 2D cases offset [left] angled [right].

C. Details of Heat Flux Formulas

(Refer to Table of Abbreviations for description of Abbreviations and Symbols)

i. Offset

$$Ld_{pv,c} = \epsilon_{pv} \cdot \sigma \cdot {T_{pv,c}}^4 \cdot Apv_c \quad (18)$$

$$Sd_{atm,c} = GHI \cdot A_3 \quad (19)$$

$$Sd_{pv,c} = ALB_c \cdot Apv_c \quad (20)$$

$$Su_c = a_{roof} \cdot Sd_{pv,c} \quad (21)$$

$$Lu_{r,c} = \epsilon_{roof} \cdot \sigma \cdot {T_{r,c}}^4 \cdot Apv_c \quad (22)$$

$$Lu_c = \epsilon_{roof} \cdot \sigma \cdot {T_{r2_c}}^4 \cdot A_3 \quad (23)$$

$$Su_{atm,c} = a_{roof} \cdot GHI \cdot A_3 \quad (24)$$

$$G_c = \left(\frac{A_3}{l}\right) \cdot k_{roof} \cdot \left(T_{r2_c} - T_{s_c}\right) \quad (25)$$

$$G_{pv,c} = \left(\frac{A_{pv}}{l}\right) \cdot k_{roof} \cdot \left(T_{r_c} - T_{s_c}\right) \quad (26)$$

$$H_c = h_{roof} \cdot \left(T_{air} - T_{r2_c}\right) \cdot A_3 \quad (27)$$

$$H_{pv,c} = h_c \cdot (T_{g_c} - T_{r_c}) \cdot Apv_c \quad (28)$$

$$Qout_c = \frac{1}{1.5692}[Ti_c - (T_{air} \cdot 1.1)] + 42.5 \quad (29)$$

ii. Angled

$$Ld_{pv,a} = \frac{1}{2}(\epsilon_{pv} + \epsilon_{atm}) \cdot \sigma \cdot {T_{pv,a}}^4 \cdot Apv_a \quad (30)$$

$$Sd_{atm,a} = GHI \cdot A_2 \quad (31)$$

$$Sd_{pv,a} = ALB_a \cdot Apv_a \quad (32)$$

$$Su_a = a_{roof} \cdot Sd_{p,v\,a} \quad (33)$$

$$Lu_{r,a} = \epsilon_{roof} \cdot \sigma \cdot {T_{r,a}}^4 \cdot Apv_a \quad (34)$$

$$Lu_a = \epsilon_{roof} \cdot \sigma \cdot {T_{r2_a}}^4 \cdot A_2 \quad (35)$$

$$Su_{atm,a} = a_{roof} \cdot GHI \cdot A_2 \quad (36)$$

$$G_a = \left(\frac{A_2}{l}\right) \cdot k_{roof} \cdot \left(T_{r2_a} - T_{s_a}\right) \quad (37)$$

$$G_{pv,a} = \left(\frac{A_{pv}}{l}\right) \cdot k_{roof} \cdot \left(T_{r_a} - T_{s_a}\right) \quad (38)$$

$$H_a = h_{roof,a} \cdot \left(T_{air} - T_{r2_a}\right) \cdot A_2 \quad (39)$$

$$H_{pv,a} = h_a \cdot (T_{g_a} - T_{r_a}) \cdot Apv_a \quad (40)$$

$$Qout_a = \frac{1}{1.5692}[Ti_a - (T_{air} \cdot 1.1)] + 42.5 \quad (41)$$

iii. Flush

$$Lu_{r,f} = \epsilon_{roof} \cdot \sigma \cdot {T_{r,f}}^4 \cdot Apv_f \quad (42)$$

$$Lu_f = \epsilon_{roof} \cdot \sigma \cdot {T_{r2_f}}^4 \cdot A_1 \quad (43)$$

$$Ld = from\ CIMIS\ (same\ for\ all) \quad (44)$$

$$Ld_{pv,f} = \epsilon_{pv} \cdot \sigma \cdot {T_{pv,f}}^4 \cdot Apv_f \quad (45)$$

$$Sd_{atm,f} = GHI \cdot A_1 \quad (46)$$

$$Su_f = a_{roof} \cdot Sd_{atm,f} \quad (47)$$

$$G_f = \left(\frac{A_1}{l}\right) \cdot k_{roof} \cdot \left(T_{r2_f} - T_{s_f}\right) \quad (48)$$

$$G_{pv,f} = \left(\frac{A_{pv}}{l}\right) \cdot k_{roof} \cdot \left(T_{r_f} - T_{s_f}\right) \quad (49)$$

$$H_f = h_{roof,f} \cdot \left(T_{air} - T_{r2_f}\right) \cdot A_1 \quad (50)$$

$$H_{pv,f} = \left(\frac{A_{pv}}{l_g}\right) \cdot k_{air} \cdot \left(T_{pv_f} - T_{r_a}\right) \quad (51)$$

$$Qout_f = \frac{1}{1.5692}\left[Ti_f - (T_{air} \cdot 1.1)\right] + 42.5 \quad (52)$$

D. Inside the Units

Figure 31: A visual inside the units to show the insulation on the walls and caulk in the corners to avoid heat release

Table 8: Properties of the High Density OSB Particleboard

Thermal Conductivity	Specific Heat	Density**
0.13 W/m*K	1,300 J/kg*K	630 kg/m^3
* Values found on WoodsideStory.com **Values measured with scale		

E. Albedo Test

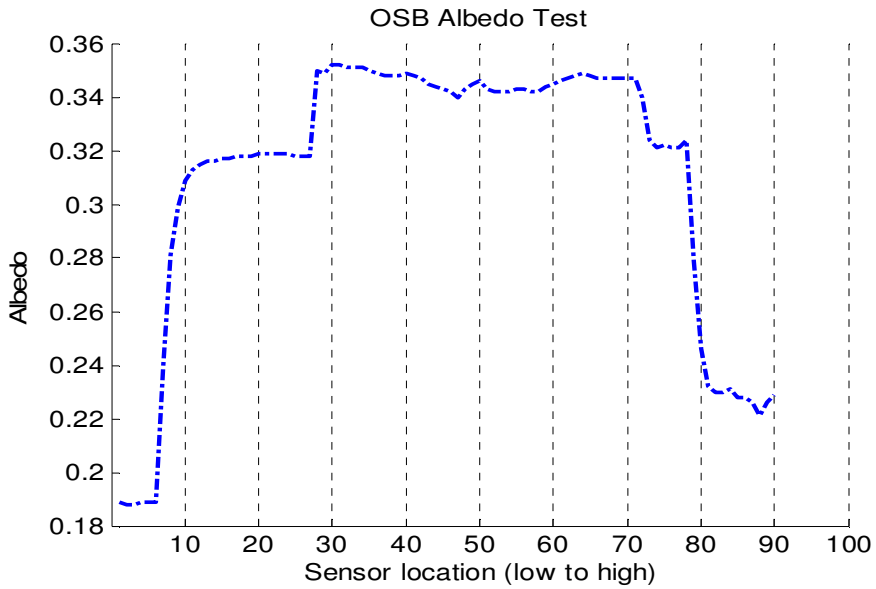

Figure 32: Albedo tests were conducted to determine the albedo of the OSB wood. The test consisted of the K&Z albedometer being brought close to the wood until shading came into effect, then far away until the ground came into effect.

F. Details of Setup #1

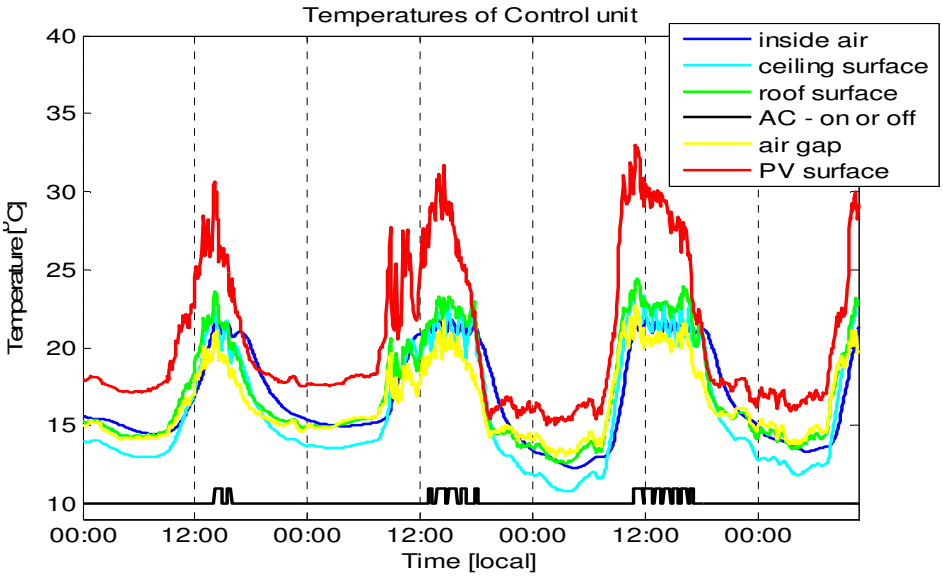

Figure 33: All the temperatures of the control unit for setup #1.

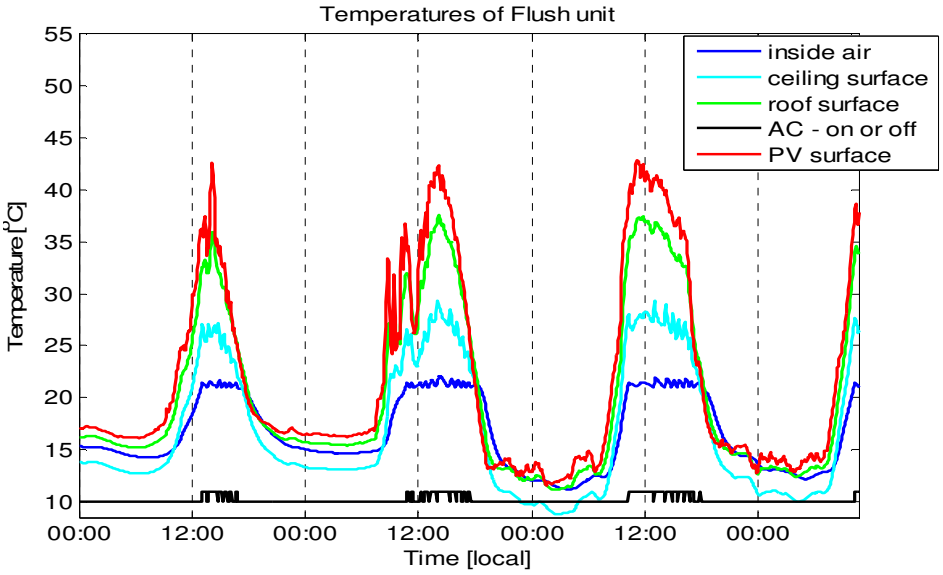

Figure 34: All the temperatures of the flush unit for setup #1.

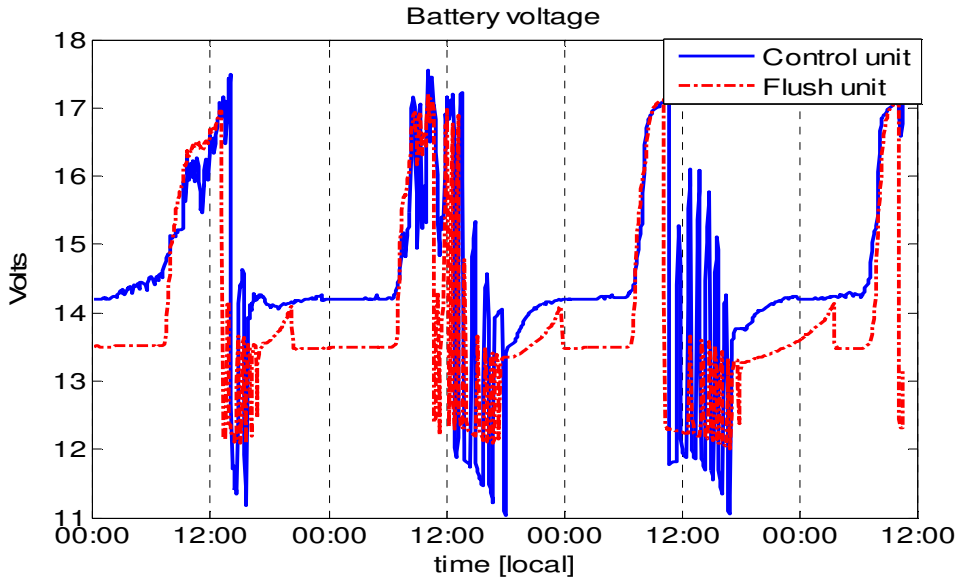

Figure 35: Battery voltage for both units of Setup #1

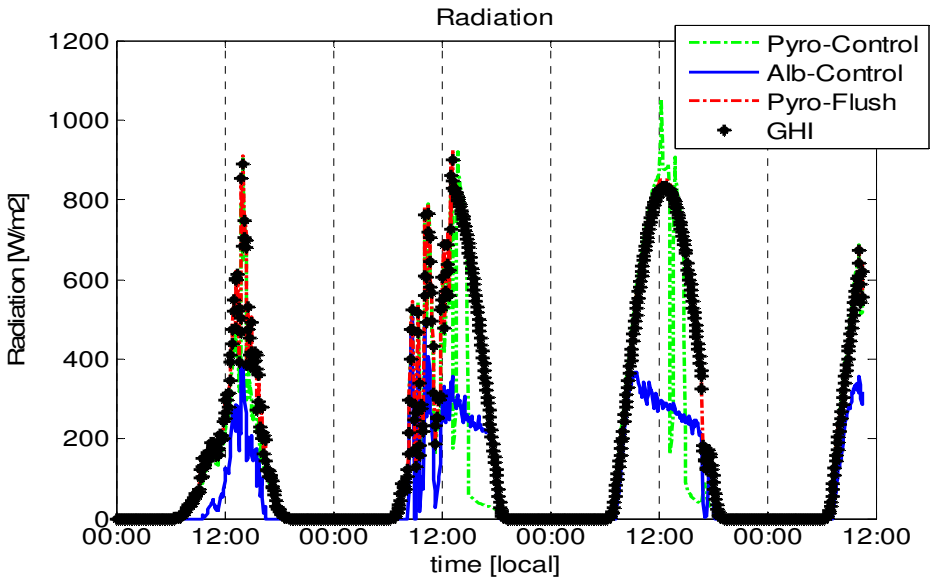

Figure 36: Radiation sensors for both units in comparison to GHI during testing days of Setup #1.

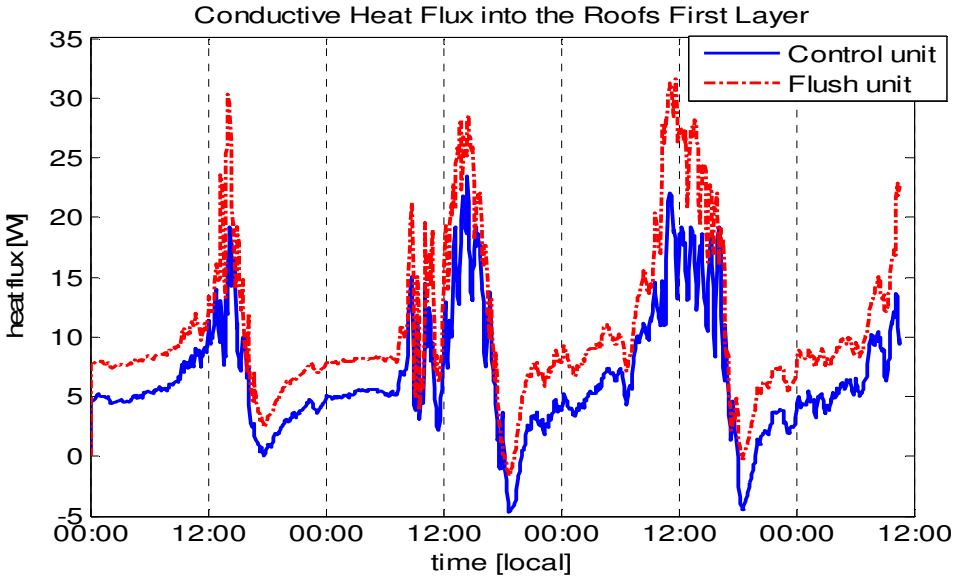

Figure 37: Conductive Heat flux in the first roof layer for both units of Setup #1

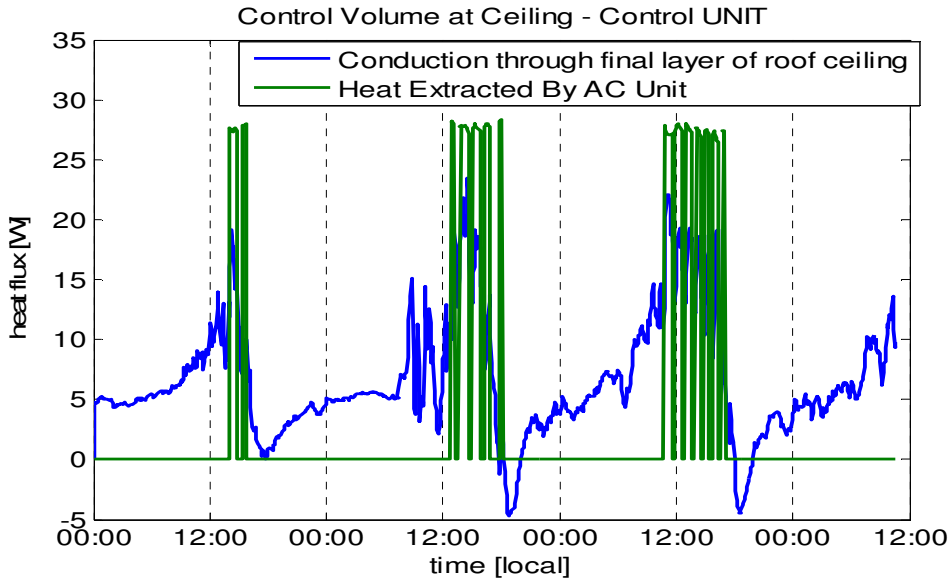

Figure 38: Energy balance of the second control volume from Figure 3 for the control unit of setup #1.

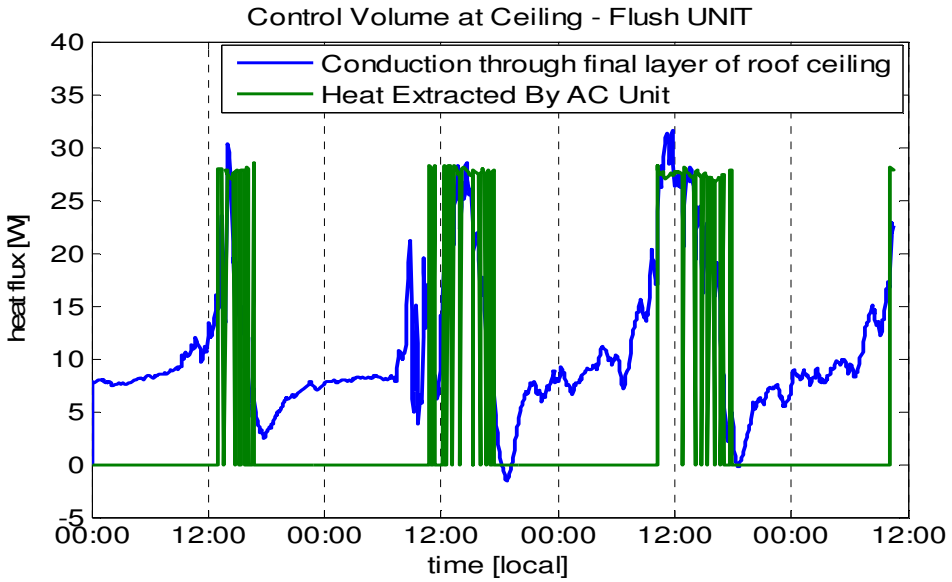

Figure 39: Energy balance of the second control volume from Figure 2 for the flush unit of setup #1.

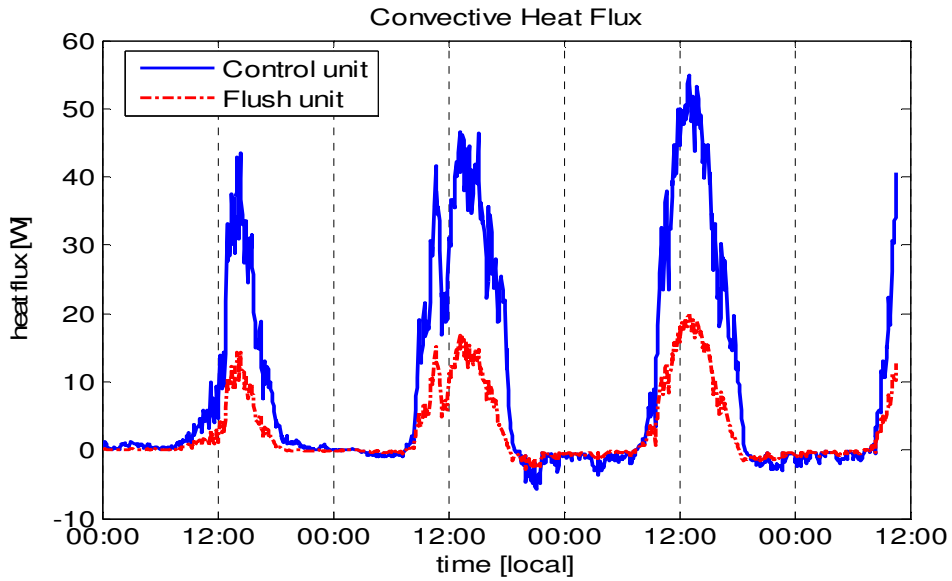

Figure 40: Comparison of the convective heat flux of the first control volume for the units of setup #1.

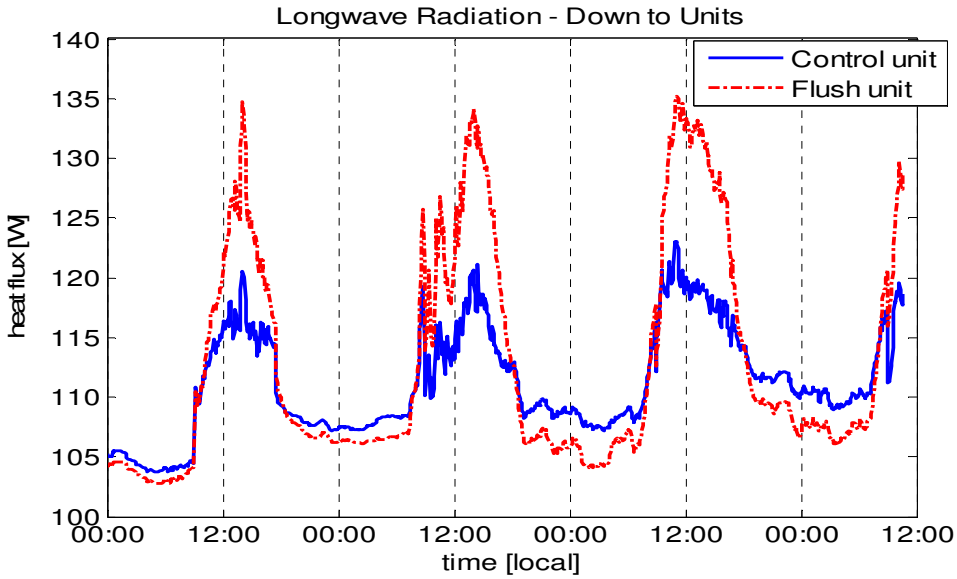

Figure 41: Comparison of the longwave radiation from the atmosphere (and solar panel for the control unit) from the first control volume for the units of setup #1.

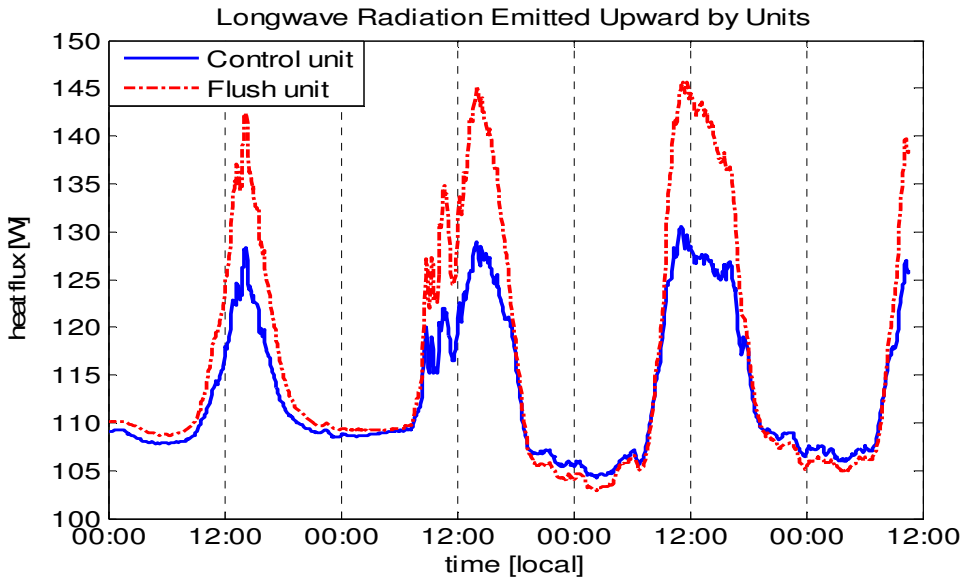

Figure 42: Comparison of the longwave radiation from the units of setup #1 up towards the atmosphere.

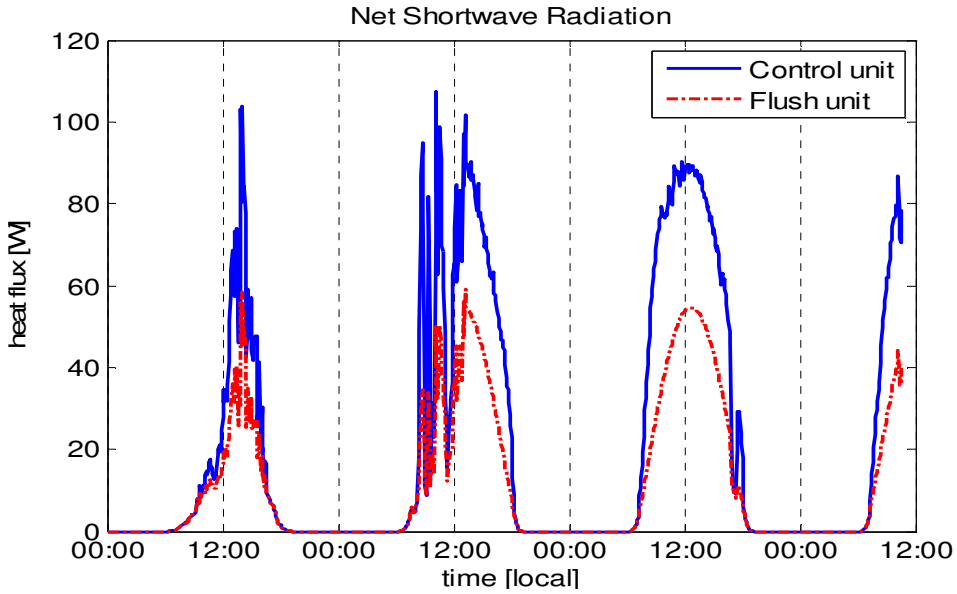

Figure 43: Comparison of the net shortwave heat flux of the first control volume for the units of setup #1. Fluxes coming up from the roof were considered positive, while shortwave down to the units was positive.

G. Details of Setup #2

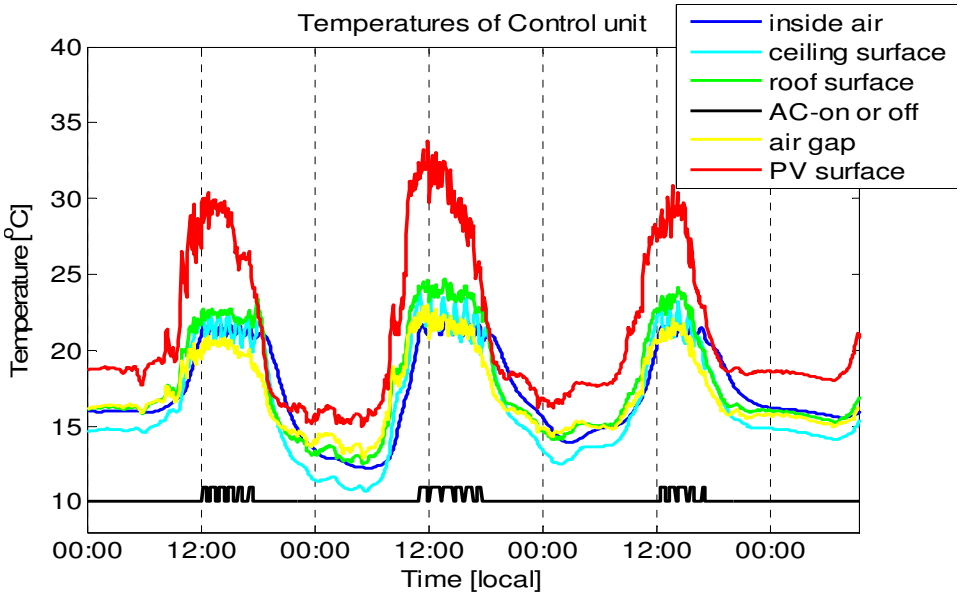

Figure 44: All the temperatures of the control unit for setup #2.

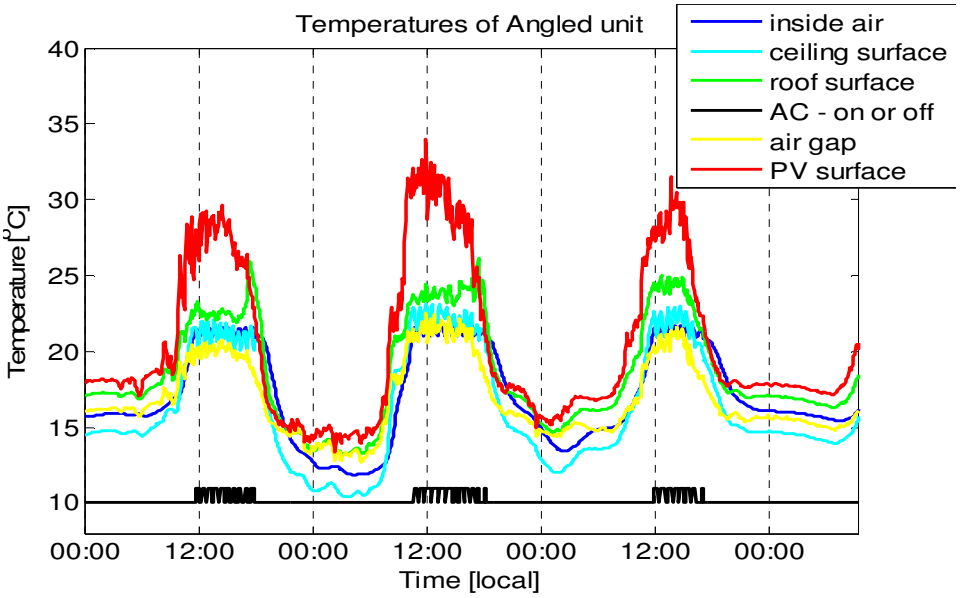

Figure 45: All the temperatures of the angled unit for setup #2.

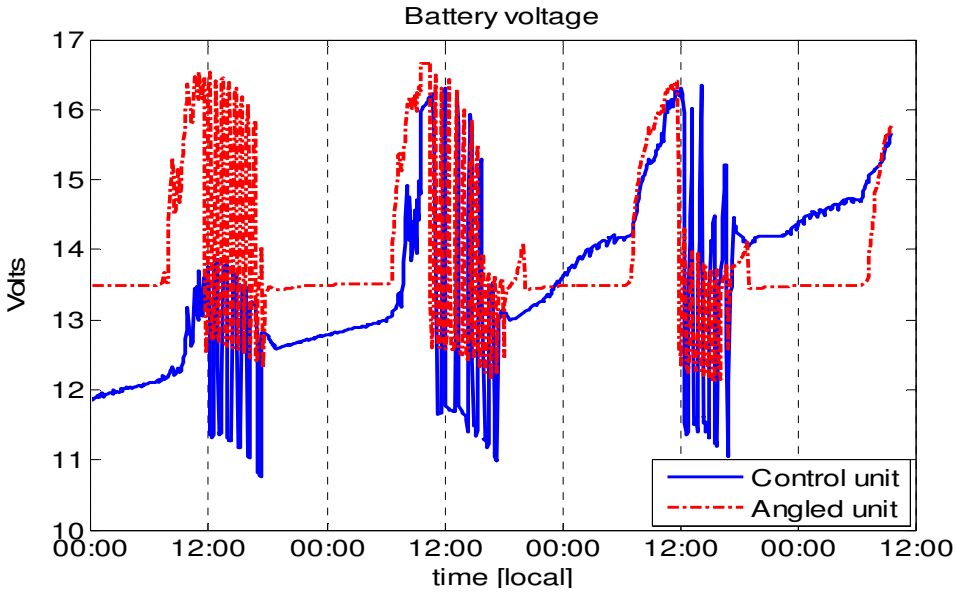

Figure 46: Battery voltage for both units of Setup #2 during the 3.5 day test.

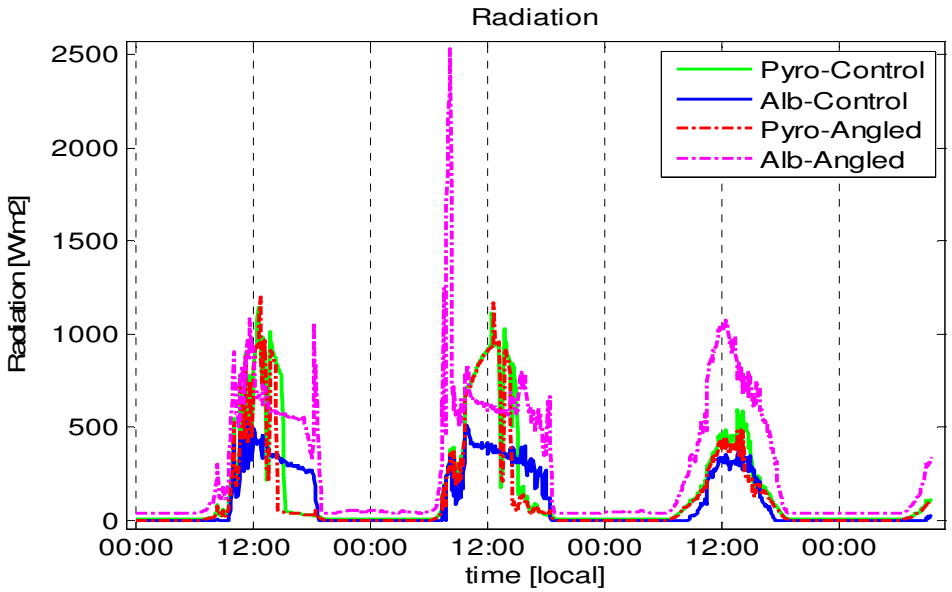

Figure 47: Comparison of the radiation sensor measurements for both units in during the testing days of Setup #2.

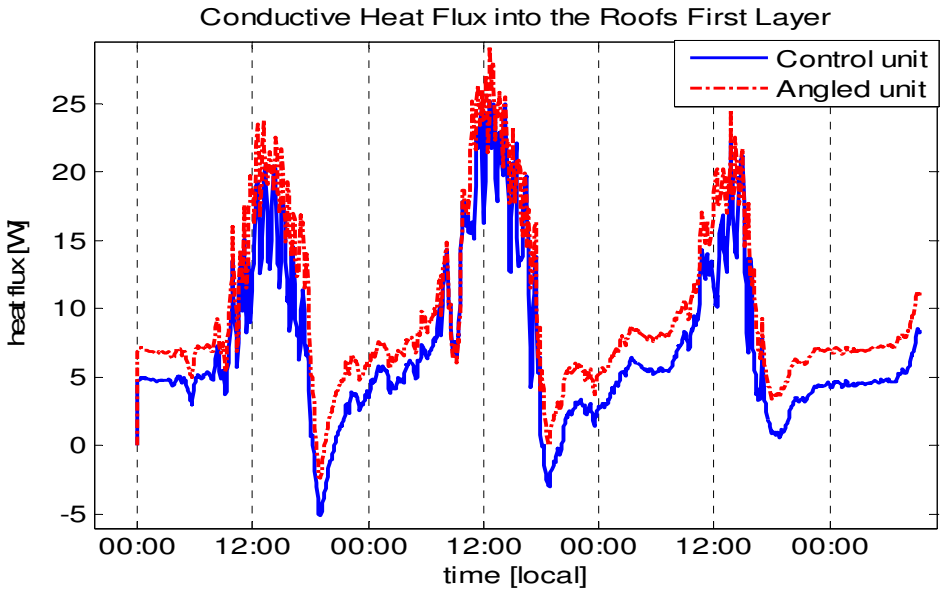

Figure 48: Conductive Heat flux in the first roof layer for both units of Setup #2.

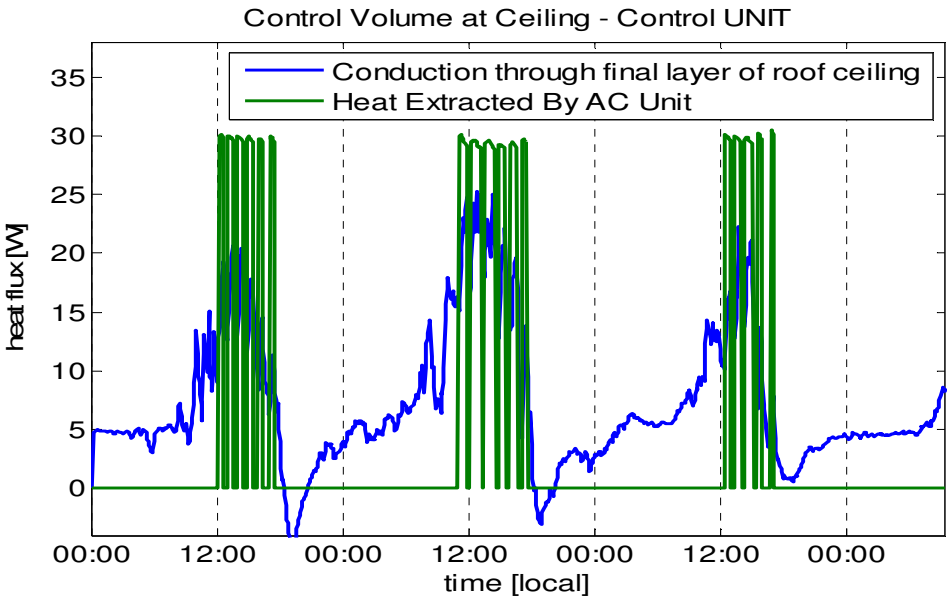

Figure 49: Energy balance of the second control volume from Figures 3 for the control unit of setup #2.

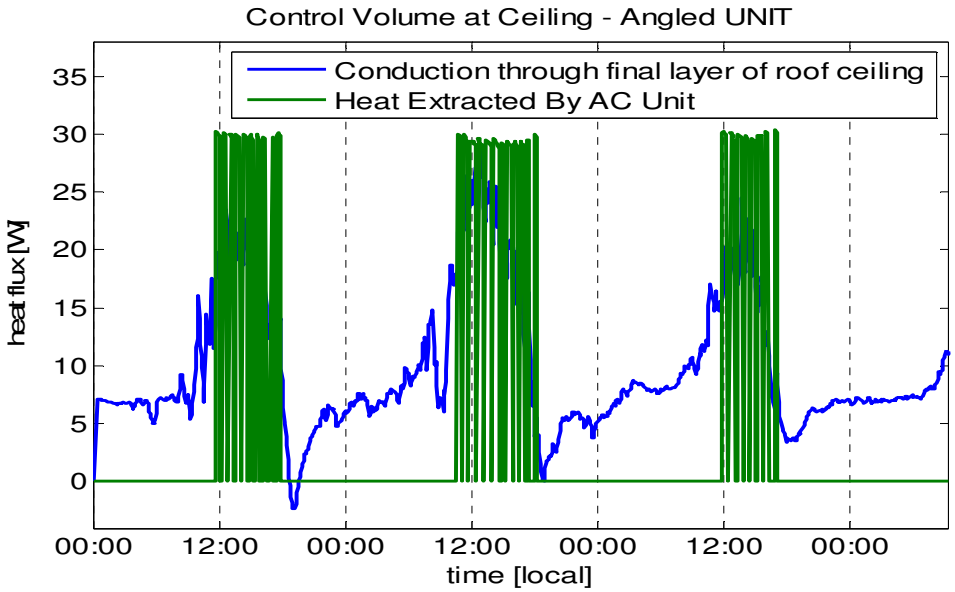

Figure 50: Energy balance of the second control volume from Figures 4 for the angled unit of setup #2.

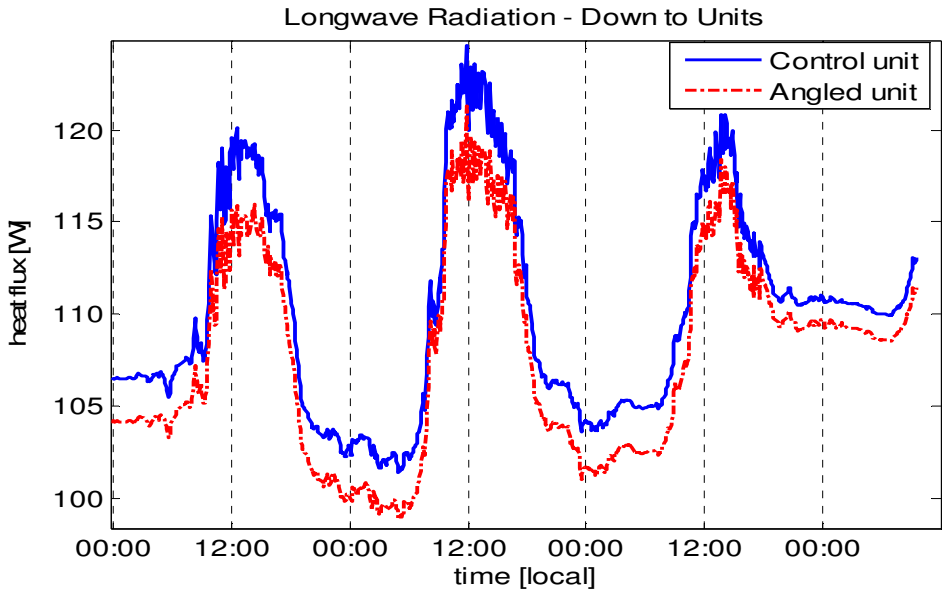

Figure 51: Comparison of the convective heat flux of the first control volume for the units of setup #2.

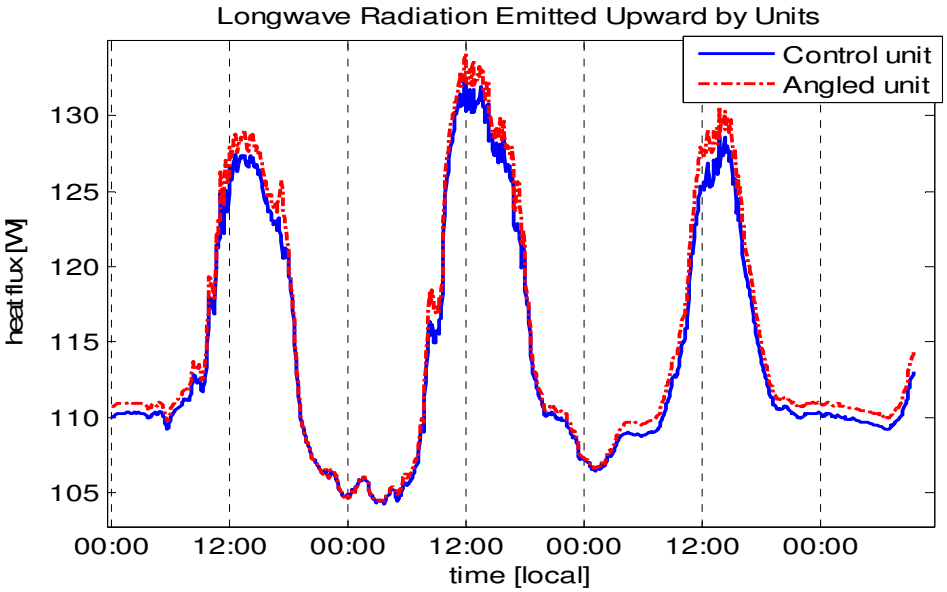

Figure 52: Comparison of the longwave radiation from the atmosphere (and solar panel for the control unit) from the first control volume for the units of setup #2.

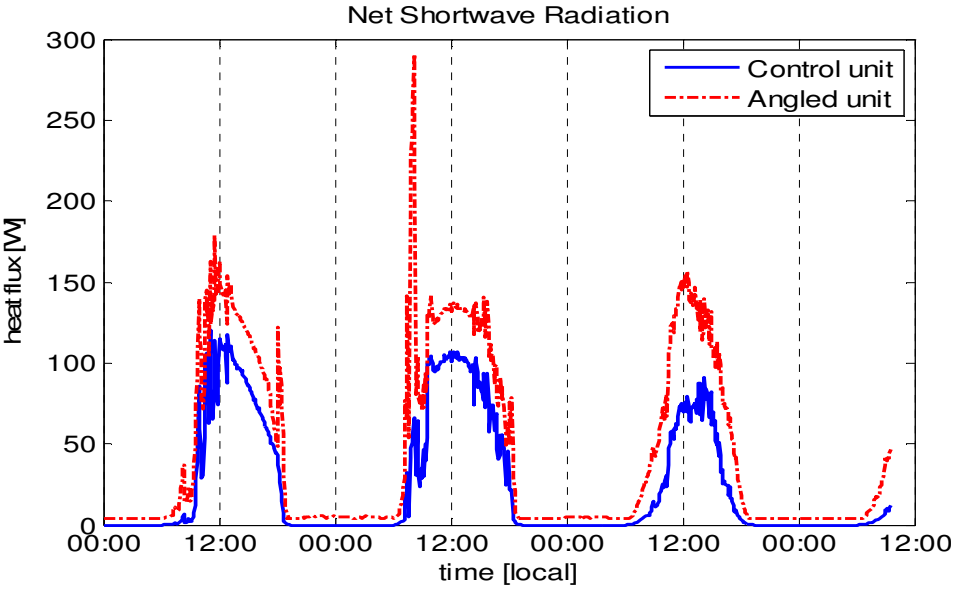

Figure 53: Comparison of the longwave radiation from the units of setup #2 up towards the atmosphere.

H. Modeled Tpv from A.D. Jones:

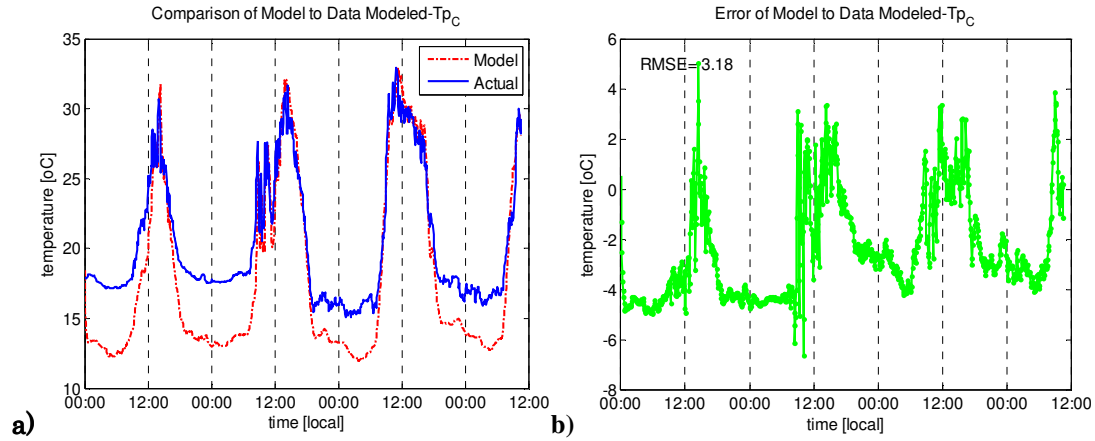

a) b)

Figure 54: a) Modeled panel temperatures for the control unit compared to the actual; b) error of the modeled panel temperature with RMSE of 3.18.

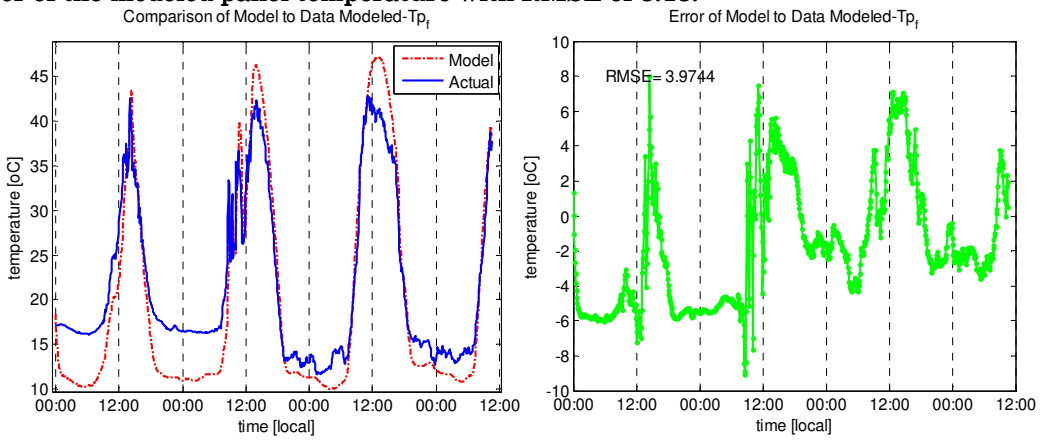

Figure 55: a) Modeled panel temperatures for the flush unit compared to the actual; b) error of the modeled panel temperature with RMSE of 3.97.

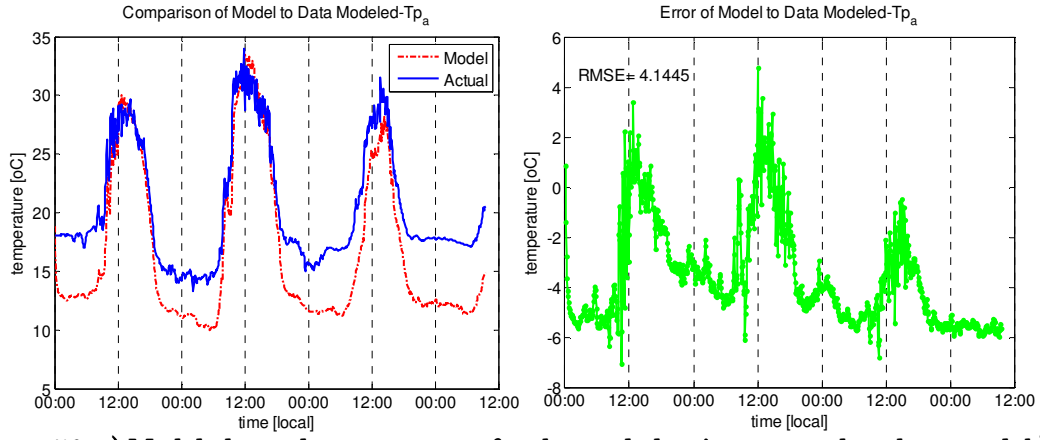

Figure 56: a) Modeled panel temperatures for the angled unit compared to the actual; b) error of the modeled panel temperature with RMSE of 4.14.

I. Modeled Temperatures using Actual Values

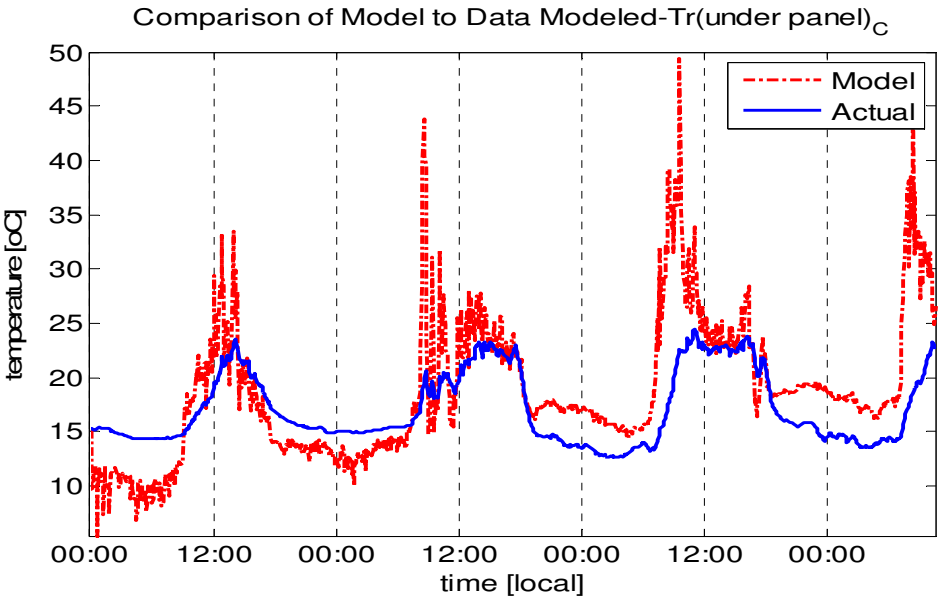

Figure 57: Modeled exposed rooftop temperatures for the control unit compared to the actual using the actual values of Tg, Tr_2 and Tp (as opposed to modeled temperatures).

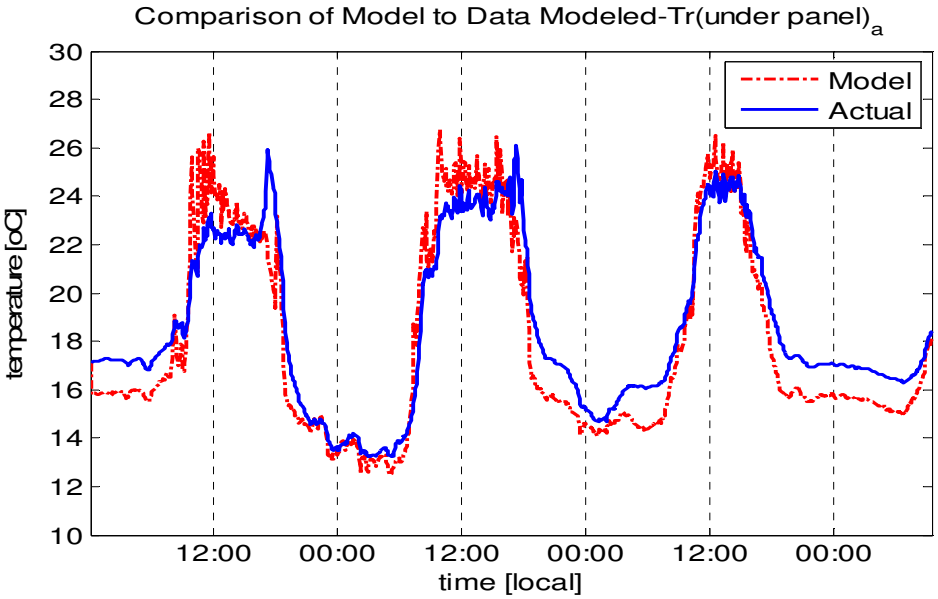

Figure 58: Modeled exposed rooftop temperatures for the angled unit compared to the actual using the actual values of Tg, Tr_2 and Tp (as opposed to modeled temperatures).

J. HVAC Operation

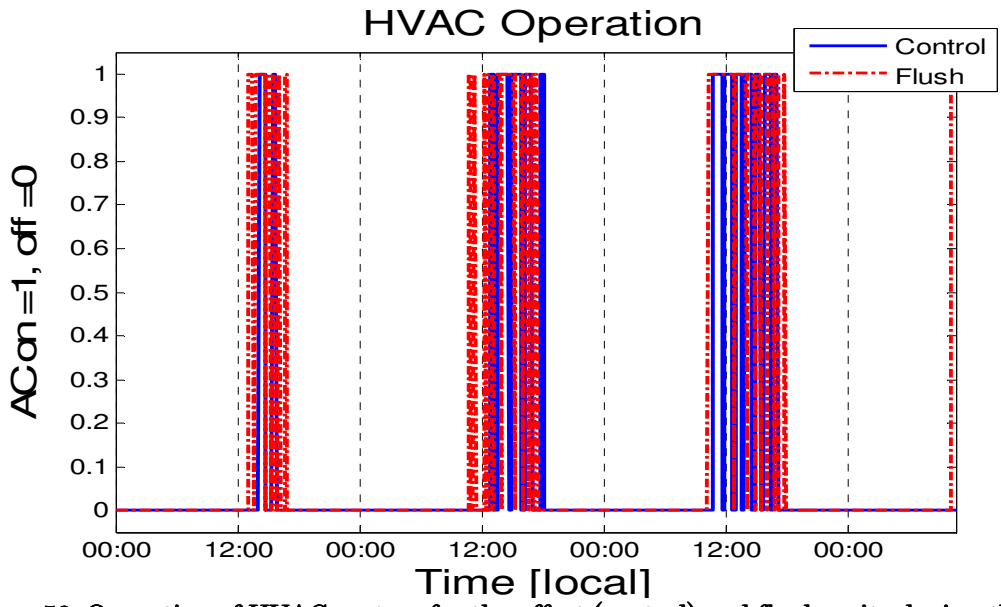

Figure 59: Operation of HVAC system for the offset (control) and flush units during the 3.5 day test of Setup #1. A value of 1 represents AC on, and a value of 0 represents AC off.

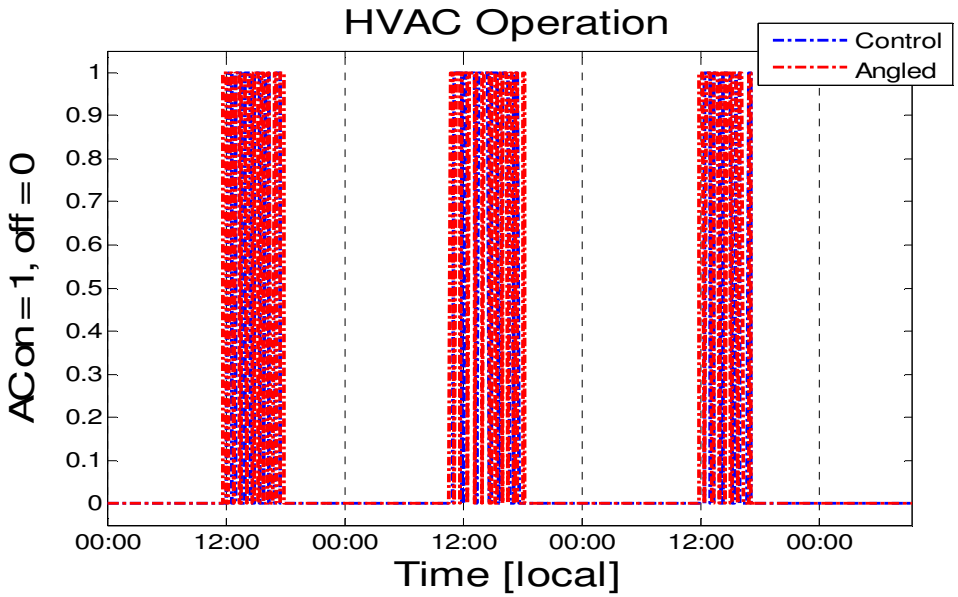

Figure 60: Operation of HVAC system for the offset (control) and angled units during the 3.5 day test of Setup #2. A value of 1 represents AC on, and a value of 0 represents AC off.

K. PVWatts Calculations

Station Identification	
City:	San Diego
State:	California
Latitude:	32.73° N
Longitude:	117.17° W
Elevation:	9 m
PV System Specifications	
DC Rating:	8.2 kW
DC to AC Derate Factor:	0.770
AC Rating:	6.3 kW
Array Type:	Fixed Tilt
Array Tilt:	32.6°
Array Azimuth:	180.0°
Energy Specifications	
Cost of Electricity:	17.4 ¢/kWh

Results			
Month	Solar Radiation (kWh/m²/day)	AC Energy (kWh)	Energy Value ($)
1	4.82	897	156.08
2	5.35	892	155.21
3	5.91	1089	189.49
4	6.53	1150	200.10
5	6.05	1108	192.79
6	5.99	1046	182.00
7	6.27	1116	194.18
8	6.62	1168	203.23
9	6.02	1037	180.44
10	5.88	1069	186.01
11	5.15	919	159.91
12	4.67	856	148.94
Year	5.77	12348	2148.55

Figure 61: Calculation of PVWatts energy output produced by the angled solar panel in La Jolla, CA. The calculation took into account the default of a 0.77 DC to AC Derate factor and an elevation of 9m. Values were first calculated for the average building then divided by the 1:800 ratio.
http://rredc.nrel.gov/solar/calculators/PVWATTS/version1/US/inputv1_us.cgi?wban=23188

Station Identification	
City:	San Diego
State:	California
Latitude:	32.73° N
Longitude:	117.17° W
Elevation:	9 m
PV System Specifications	
DC Rating:	8.2 kW
DC to AC Derate Factor:	0.770
AC Rating:	6.3 kW
Array Type:	Fixed Tilt
Array Tilt:	0.0°
Array Azimuth:	180.0°
Energy Specifications	
Cost of Electricity:	17.4 ¢/kWh

Results			
Month	Solar Radiation (kWh/m²/day)	AC Energy (kWh)	Energy Value ($)
1	3.13	557	96.92
2	3.93	645	112.23
3	5.04	934	162.52
4	6.31	1119	194.71
5	6.38	1178	204.97
6	6.63	1169	203.41
7	6.81	1228	213.67
8	6.59	1175	204.45
9	5.36	928	161.47
10	4.46	804	139.90
11	3.41	591	102.83
12	2.87	498	86.65
Year	5.08	10828	1884.07

Figure 62: Calculation of PVWatts energy output produced by the flush and offset solar panel in La Jolla, CA. The calculation took into account the default of a 0.77 DC to AC Derate factor and an elevation of 9m.Values were first calculated for the average building then divided by the 1:800 ratio.
http://rredc.nrel.gov/solar/calculators/PVWATTS/version1/US/inputv1_us.cgi?wban=23188